A two-dimensional Fourier transform electron-spin resonance (ESR) study of nuclear modulation and spin relaxation in irradiated malonic acid

Sanghyuk Lee, Baldev R. Patyal, and Jack H. Freed
Baker Laboratory of Chemistry, Cornell University, Ithaca, New York 14853

(Received 18 September 1992; accepted 17 November 1992)

Nuclear modulation in electron-spin-echo spectroscopy is conventionally studied by one-dimensional electron-spin-echo envelope modulation (1D-ESEEM). Two-dimensional Fourier transform electron-spin resonance (2D-FTESR) studies of nuclear modulation have the promise of enhancing the spectral resolution and clarifying the key details of the relaxation processes. We present a 2D-FTESR study on single proton nuclear modulation from γ-irradiated malonic acid single crystals to test the validity of the Gamliel–Freed theory and to assess the value of the new methods. The two pulse spin-echo correlation spectroscopy (SECSY) spectra as a function of orientation of the single crystal show very good agreement with the Gamliel–Freed theory extended to the general case of nonaxially symmetric hyperfine interaction. It is very simply affected by spin relaxation, such that relative intensities are essentially unaffected. Thus SECSY-ESR can most reliably be utilized for studying nuclear modulation. Stimulated SECSY provides the simplest nuclear modulation patterns, which, however, do exhibit the suppression effect well known in three-pulse ESEEM studies. Two-dimensional electron–electron double resonance (2D-ELDOR) provides nuclear modulation patterns similar to that of SECSY-ESR, so the suppression effect is absent. Both three-pulse methods exhibit complex relaxation behavior which can affect relative intensities. This is a feature characteristic of three-pulse ESEEM, but is not well understood. It is shown how the 2D-FTESR methods enable one to obtain the details of the complex spin relaxation, and in the process, obtain very good agreement between experiment and theory. 2D-ELDOR exhibits exchange cross peaks as well as coherence peaks from the nuclear modulation. It is shown how experiments, as a function of mixing time, enable one to separate the effects of the two. It is pointed out that such experiments are in the spirit of 3D spectroscopy. A new observation of the broadening of the 2D-ELDOR main peaks with an increase in mixing time is ascribed to the effects of solid-state dynamical processes that are slow on the ESR time scale and may thus be studied in "real time" in such experiments. The analysis of spin relaxation in this study is enabled by a full Liouville space derivation of the combined effects of nuclear modulation and spin relaxation in 2D-FTESR.

I. INTRODUCTION

Nuclear modulation of the electron-spin-echo decay was first reported in 1961[1,2] and thereafter was developed both theoretically and experimentally in the context of electron-spin-echo envelope modulation (ESEEM).[3,4] ESEEM has been studied over the ensuing years with the objective of obtaining structural information near paramagnetic centers in solid and glassy matrices.[5–10] This method has been most successful in dealing with nuclei that are weakly coupled to the electron spin by dipolar interactions. In these cases, the depth of the ESEEM can be exploited to estimate distances between the nuclei and the unpaired electron. Given that the ESEEM usually observed is due to weakly interacting nuclei, the structural information that is obtained is typically complementary to that obtained from electron-nuclear double resonance (ENDOR).[6,11–14]

An important recent development in electron-spin resonance (ESR) has been Fourier transform (FT) and two-dimensional FT-ESR (2D-FT-ESR).[15–22] These developments have the technical advantages of (a) greatly reduced data acquisition times because the whole spectrum is irradiated simultaneously (i.e., the multiplex advantage) with the use of very narrow nonselective pulses (widths ~ 5 ns) which are significantly shorter than the relevant T_2's, thereby yielding (b) reduced dead time and spectral distortions arising from the use of long pulses. More important is the availability of a whole class of new experiments to study both motions and structure. In this paper, we address the class of 2D-FT-ESR experiments for the study of nuclear modulation.

In a recent theoretical study by Gamliel and Freed (GF),[23] it was shown that 2D-FT-ESR methods should, in general, provide greater spectral resolution of nuclear modulation with the availability of the second spectral dimension. In fact, the first demonstration of the value of a second spectral dimension in the study of ESEEM was provided by Merks and de Beer.[24] They utilized a standard ESEEM technique based on the three-pulse stimulated echo, which measures just the echo maximum as a function of two different pulse delay times [T and t_1 in Fig. 1(d)]. Also notable was the two-pulse ESEEM experiment of Isoya *et al.*[25] who measured the echo maximum as a func-

 0021-9606/93/053665-25$06.00

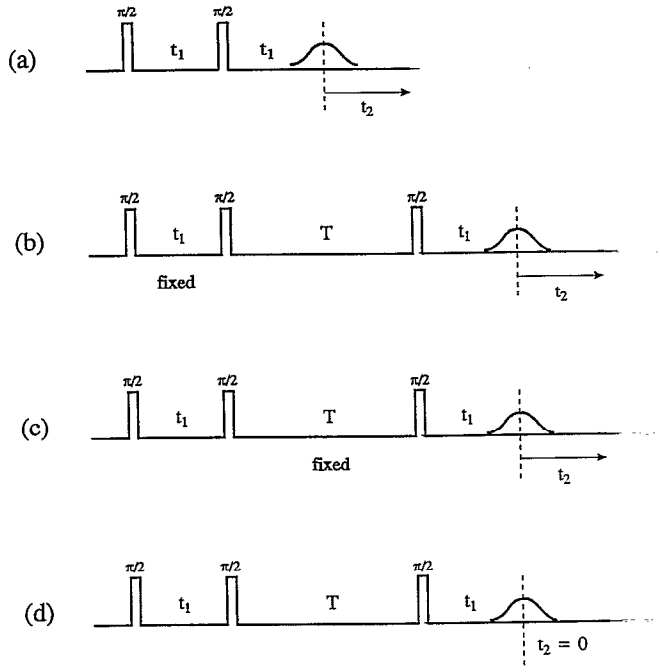

FIG. 1. The 2D-FTESR pulse sequences for echo signals: (a) SECSY—one varies t_1 and t_2; (b) stimulated SECSY—one varies T and t_2 with fixed t_1; (c) echo-ELDOR—one varies t_1 and t_2 with fixed mixing time T; (d) Merks–de Beer 2D-ESEEM experiment—one varies t_1 and T and monitors the echo height.

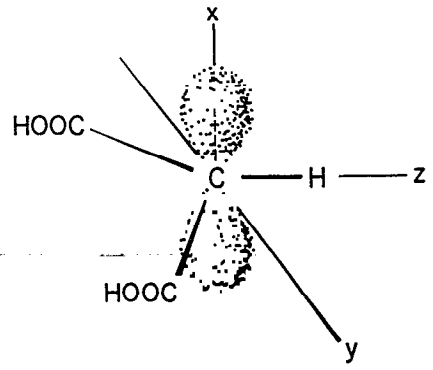

FIG. 2. Relation of the structure of the malonic acid radical $\cdot CH(COOH)_2$ to the principal axes (x,y,z) of the hyperfine tensor. In this orthogonal system of coordinates, the z axis is along the CH bond direction and the x axis is perpendicular to the plane of the three carbon atoms (Ref. 30). The direction of the external static field H_0 is defined by the angles θ and ϕ, where θ is the angle between H_0 and the z axis, and ϕ is the angle between the x axis and the projection of H_0 on the xy plane.

tion of t_1 [cf. Fig. 1(a)] and repeated the experiment for different values of the d.c. magnetic field B_0 to obtain a two-dimensional representation. These techniques are based on selective excitation and/or detection and do not have the multiplex advantage of a technique based on modern FT methodology. We distinguish the methods described in this paper by their full utilization of nonselective irradiation and their use of modern FT methods.

Patyal *et al.*[26,27] have recently demonstrated the capability of performing 2D-FT-ESR on spectra in the rigid and near rigid limits in a disordered matrix. They employed the GF theory to interpret the 2D nuclear modulation observed from a nitroxide in a glycerol/H_2O host and showed the sensitivity of the 2D-FT-ESR methods to structural detail. It is known that rotational motions significantly affect nuclear modulation,[19,20,26–28] and Patyal *et al.* were able to illustrate these effects in their 2D-FT-ESR. In general, relaxation mechanisms can affect the observed nuclear modulations in terms of intensities and resolution, a matter that is still not well understood.

In this paper, we present a study of 2D-FT-ESR experiments on the nuclear modulation from a γ-irradiated single crystal of malonic acid (Fig. 2). This is meant as a prototype study to carefully demonstrate and analyze the capabilities of 2D-FT-ESR experiments in the study of nuclear modulation. The reasons for choosing the malonic acid radical are that (i) it is a simple $S=1/2$, $I=1/2$ spin system, which is easy to analyze; and (ii) detailed structural information is available by x-ray crystallography[29] and from previous ESR studies.[30,31] We are able to study the various 2D-FT-ESR spectra as a function of sample orientation, which leads to dramatic variation of the observed nuclear modulation in a way that provides an excellent test of the theory. We are able to report on the generally excellent agreement obtained with GF theory after generalizing it to include nonaxially symmetric hyperfine (and g) tensors.

This work also illustrates another virtue of our 2D-FT-ESR methods with short nonselective pulses, viz., it is possible to obtain good nuclear modulation from strongly coupled nuclei such as is the case for the α proton in malonic acid. In order to perform accurate studies on nuclear modulation, it is necessary to excite the allowed and forbidden ESR transitions simultaneously. Their difference in frequency depends on both the hyperfine (hf) tensor and the nuclear Larmour frequency ω_n. In general, it is difficult to adequately excite nuclear modulation of protons because ω_n is large, but Patyal *et al.* showed that 5 ns pulses were adequate to accomplish this in the case of relatively weakly coupled protons,[26,27] and in the present work, we find that this is so for a strongly coupled proton where all principal components of the hf tensor are greater than ω_n. Thus 2D-FT-ESR can deal effectively with weakly and strongly coupled nuclei including protons.

In this paper, we consider three canonical 2D-FT-ESR experiments that are based on echo decays. The first is the two-pulse spin-echo correlation spectroscopy (SECSY)-ESR experiment in which one collects the full echo decay as one steps out the time t_1 between the two pulses [cf. Fig. 1(a)] followed by a double FT.[23,26] This technique leads to coherence cross peaks due to the nuclear modulation. These coherence cross peaks are analogous to those observed in COSY (correlation spectroscopy) and SECSY NMR arising from jj coupling,[32] although the formulation of nuclear modulation in ESR is more complex. This is the basic experiment which generalizes the standard two-pulse ESEEM experiment to two dimensions. There are two

three-pulse 2D-FT-ESR experiments which are based on the stimulated echo—stimulated SECSY [cf. Fig. 1(b)] and 2D-electron–electron double resonance (ELDOR)-echoes [cf. Fig. 1(c)]. Since there are actually three different times here, viz. t_1 the preparation time, T the mixing time, and t_2 the acquisition time, this is, in principle a 3D experiment.[33] The 2D experiments—stimulated SECSY (in which T and t_2 are "varied") and 2D-ELDOR (in which t_1 and t_2 are varied) are two of the three possible 2D projections of the full 3D experiment. The third is, of course, the Merks and de Beer experiment (t_1 and T is varied), but it is the one that lacks the multiplex advantages referred to above. One finds that echo-ELDOR for short mixing times, T yields results very similar to SECSY-ESR for the structure of the coherence cross-peaks due to nuclear modulation. As T increases, cross peaks due to exchange processes can be observed to grow in. We consider, in our study, how coherence cross peaks and exchange cross peaks can be distinguished by such experiments. In general, stimulated SECSY and 2D-ELDOR are more sensitive to the details of spin relaxation than is SECSY. In the original GF theory, relaxation was treated in a very simple manner in order to avoid the full Liouville space analysis required for a relaxation-matrix[34] or a stochastic-Liouville equation[33] treatment of the ESR. The nuclear-modulation problem (ignoring detailed spin relaxation) is adequately dealt with in the normal Hilbert space spanned by the spin basis functions as Mims has shown. In order to properly analyze the combined effects of nuclear modulation and spin relaxation required for the present 2D-ESR experiments (as well as conventional 1D ESEEM), we have recast the theory including relaxation in the full Liouville space. This has enabled us to properly assess how electron-spin relaxation, nuclear spin relaxation, and cross-relaxation affect the 2D spectra. We thereby indicate how such 2D-ESR experiments can provide both relaxation and structural information on radicals in a solid host.

In Sec. II, the experimental details are presented. The appropriate theory for these experiments is summarized in Sec. III, with a more detailed description of the derivation including spin relaxation given in the appendices. The results and discussion appear in Sec. IV and the conclusions are given in Sec. V.

II. EXPERIMENT

All the experiments were performed on the 2D-FT-ESR spectrometer, which has been described elsewhere.[16,20] Additional modifications, as well as the bridged loop gap resonator (BLGR) utilized have been described by Patyal *et al.*[26] The use of a resonator with low $Q \approx 45$ as well as short $\pi/2$ pulses (~ 5 ns) permits wide-band coverage. In this work, we were able to achieve nearly uniform rotation of spins into the rotating xy plane over a ± 100 MHz bandwidth. This coverage is more than sufficient for the present study where the largest hf tensor component $A_{yy}=91$ MHz.

A significant increase in the rate of data acquisition was achieved over the previous studies by utilizing a computer-aided measurement and control (CAMAC) dual channel digitizer and averager (DSP Technology TRAQ-H model 2102SA) which samples at the rate of 200 megasamples/s (i.e., 5 ns dwell time). It was interfaced with a home-built synchronized clock, which allows for interleaving in successive sweeps to achieve an effective 1 ns resolution when needed. In the experiments reported here, we utilized a sweep rate of 1000 sweeps/s (for 256 data points). This yielded a total throughput rate of data acquisition that was about 15 times faster than we previously obtained using an HP54100A digitizing oscilloscope. Additional improvements, since completing these experiments, now permit sweep rates of 10 000 sweeps/s under otherwise identical conditions for an increase by about a factor of 150 over our original throughput rate.

Malonic acid crystals grown previously in our laboratory were used in this study. Some crystals were irradiated with 1 Mrad ^{60}Co γ radiation at the Ward Laboratory of Nuclear Engineering at Cornell University. A crystal of ~ 2 mm $\times 1$ mm $\times 0.5$ mm, weighing 1.7 mg with well-defined faces and edges was used for data collection. Soon after irradiation, the cw-ESR spectrum shows several hf lines due to different kinds of radicals produced, but in aged samples (a couple of days after irradiation), only two strong lines persist. The strong doublet is due to the hf coupling of the π electron of the α carbon with the α proton of the C–H fragment of the $\cdot CH(COOH)_2$ radical of malonic acid.

The principal axis system of the hf tensor defined in Ref. 30 and the procedure to identify the axes described therein were used in this study. Figure 2 shows the principal axes (x,y,z) of the hf tensor in relation to the structure of the malonic acid radical $\cdot CH(COOH)_2$. The direction of the external static field B_0 is defined by the angles θ and ϕ, where θ is the angle between B_0 and the z axis, and ϕ is the angle between the x axis and the projection of B_0 on the xy plane. The crystal was mounted on a specially designed delrin holder which was connected to a glass rod (~ 2.5 mm diameter). The other end of the glass rod was attached to a goniometer. The crystal was rotated successively about one of the three principal axes (x,y,z) and measurements were made at several orientations.

At room temperature T_2^* is too short to allow the detection of a free induction decay (FID), but an echo decay can be easily measured. Figure 1 shows three types of experiments performed at each orientation. For the two-pulse SECSY-ESR experiment, the initial t_1 was 110 ns due to the spectrometer dead time and 128 steps along t_1 were used. The t_1 step size was set either 5 or 10 ns depending on the spectral extent required for the nuclear modulation components which appear with respect to ω_1. [That is, 5 (10) ns supplied a spectral extent of ± 100 (± 50) MHz after FFT.] For each t_1 step, the echo decay was collected along t_2, sampling 256 data points at a 1 ns interval. One important difference between our 2D technique and the conventional ESEEM is that we collect the echo shape starting at the peak of the echo as a function of t_2 for each

t_1 value, which enables us to get the cw spectrum along ω_2 after Fourier transform.

In the three pulse stimulated-SECSY experiment, the evolution period t_1 is kept constant and the mixing period T is stepped out; for each step in T, the stimulated echo was collected as a function of t_2. The initial T was 110 ns and 128 T steps of either 5 or 250 ns step size were used. The larger step size supplied a $T_{max}=32$ μs which was needed for an accurate measurement of $T_1=15$–22 μs, the electron-spin lattice relaxation time, whereas the smaller step size (5 ns) was used to obtain sufficient spectral range (± 100 MHz) required for the nuclear modulation components. In the echo-ELDOR experiment, the mixing period T is kept constant and the evolution period t_1 is stepped out; for each step in t_1, the echo decay is collected as a function of t_2. The initial t_1 was 110 or 130 ns depending on the signal to noise ratio. Here too 128 t_1 steps of 5 ns step size were used. At each orientation, three to five experiments were done for different values of the mixing time T to see any development of cross peaks as T increased.

Throughout all experiments, the phase cycling sequences suggested in Ref. 23 were used to remove the image peaks, transverse signals, and axial peaks. For example, the irradiated malonic acid crystal has five echo signals with comparable intensity in the three-pulse experiment. We could collect the stimulated echo signal selectively with phase cycling. Also, the S_{c-} spectral combination[23] of the dual quadrature signal was used in the data processing, as is appropriate for an echo signal.

The data acquisition and processing methods are described in Refs. 26 and 27. The full 2D figures shown below were obtained directly by 2D-FFT of the original time-domain data and are the magnitude spectra. These data were also processed by linear prediction with singular value decomposition (LPSVD)[20] in order to get accurate relaxation times and frequencies as needed, and to enable us to produce contour plots of just the modulation peaks from the α proton of malonic acid. The characteristic decay constants along t_1 (SECSY) or T (stimulated SECSY) are summarized in Table I.

TABLE I. Characteristic relaxation constants for each orientation.

Orientation (θ,ϕ)	T_2 (ns)[a]	Decay constants along T (μs)[b]
(5°,0°)	800	23.0
(30°,0°)	812	21.1
(50°,0°)	687	15.9
(5°,90°)	1223	22.2
(45°,90°)	1068	22.1

[a]T_2 is measured from SECSY experiment with 10 ns t_1 step size.
[b]The decay constants along mixing time are measured from stimulated-SECSY experiments with 250 ns T step size.

III. THEORY

The Gamliel–Freed theory was developed to calculate the 2D-ESR spectra in the rigid limit.[23] In this work, in order to deal properly with the 2D-ESR spectra from irradiated malonic acid, we extend the theory to include molecules with nonaxially symmetric g and hf tensors. We also include relaxation processes in a more explicit and detailed fashion.

In the general case, there is no axial symmetry in any of the tensors and the various tensors have a different principal axis system of their own. This general situation is summarized in the Schneider–Freed "User's Guide."[35] The following definitions will be used:

$$\bar{g}=\frac{1}{3}(g_{xx}+g_{yy}+g_{zz})\frac{\beta_e B_0}{\hbar},\quad \bar{a}_i=\frac{1}{3}(A^i_{xx}+A^i_{yy}+A^i_{zz}),$$

$$F=\frac{2}{3}\left[g_{zz}-\frac{1}{2}(g_{xx}+g_{yy})\right]\frac{\beta_e B_0}{\hbar},$$

$$D_i=\frac{2}{3}\left[A^i_{zz}-\frac{1}{2}(A^i_{xx}+A^i_{yy})\right], \tag{1}$$

$$F^{(2)}=\frac{1}{2}(g_{xx}-g_{yy})\frac{\beta_e B_0}{\hbar},\quad D^{(2)}_i=\frac{1}{2}(A^i_{xx}-A^i_{yy}),$$

where i is the index for the ith nucleus.

In high fields, the contribution of the nonsecular terms ($S_{\pm}$, $S_{\pm}I_z$, $S_{\pm}I_{\pm}$, $S_{\pm}I_{\mp}$) is relatively small, so one need only use the secular and pseudosecular terms to determine the spectrum. Then the Hamiltonian in the case of one electron and several nuclei can be written as follows:

$$\hat{H}=\left[\bar{g}+F\frac{1}{2}(3\cos^2\beta-1)+F^{(2)}\sin^2\beta\cos(2\gamma)\right]S_z-\sum_i\omega_{ni}I_{zi}-\sum_i\frac{\gamma_e}{\hbar}\left\{\left[\bar{a}_i+D_i\frac{1}{2}(3\cos^2\beta^i-1)\right.\right.$$
$$\left.+D^{(2)}_i\sin^2\beta^i\cos(2\gamma^i)\right]S_zI_{zi}+\left[D_i\frac{3}{4}\sin\beta^i\cos\beta^i-D^{(2)}_i\frac{1}{2}\sin\beta^i\{\cos\beta^i\cos(2\gamma^i)-i\sin(2\gamma^i)\}\right]S_zI_{+i}$$
$$\left.+\left[D_i\frac{3}{4}\sin\beta^i\cos\beta^i-D^{(2)}_i\frac{1}{2}\sin\beta^i\{\cos\beta^i\cos(2\gamma^i)+i\sin(2\gamma^i)\}\right]S_zI_{-i}\right\}, \tag{2}$$

where $\Omega=(0,\beta,\gamma)$ represents the set of Euler angles describing the orientation of the g tensor relative to a laboratory-fixed frame and $(\alpha^i,\beta^i,\gamma^i)$ are the Euler angles for the ith hf tensor. The spin operators are written in the lab frame. For the special case of a single nucleus interacting with the unpaired electron with the hf tensor having the same principal axes as the g tensor, the Hamiltonian is

$$\hat{H}=CS_z-\omega_n I_z+AS_zI_z+\tfrac{1}{2}BS_zI_+ +\tfrac{1}{2}B^*S_zI_- . \tag{3}$$

The coefficients in the Hamiltonian are now equal to

$$C=\bar{g}+F\tfrac{1}{2}(3\cos^2\beta-1)+F^{(2)}\sin^2\beta\cos(2\gamma),$$

$$A=-\frac{\gamma_e}{\hbar}\left[\bar{a}+D\tfrac{1}{2}(3\cos^2\beta-1)+D^{(2)}\sin^2\beta\cos(2\gamma)\right],$$

$$B=-\frac{\gamma_e}{\hbar}\{D\tfrac{3}{4}\sin\beta\cos\beta-D^{(2)}\tfrac{1}{2}\sin\beta[\cos\beta\cos(2\gamma)$$

$$-i\sin(2\gamma)]\}. \tag{4}$$

This is the form we specifically employ for irradiated malonic acid. Equation (3) is the typical form utilized by GF, but now the anisotropic tensor components appear in the coefficients A, B, and C as given in Eq. (4). With this modest change, the GF theory again applies provided one is not interested in details of the spin relaxation.

GF included relaxation in an extremely simple fashion to avoid the necessity of dealing with the density matrix in the full Liouville space. Such a simplification permits one to treat the effects of the various nuclear spins in an additive fashion, as Mims has shown. A detailed analysis of relaxation, however, does require a full Liouville space analysis especially for dealing with cross-relaxation, exchange cross peaks in 2D-ESR, and also to distinguish the various T_2's for the ESR and the NMR transitions. This complex matter is described in Appendix A for the case of an $S=1/2$, $I=1/2$ spin system, and an analytic analysis is provided after some simplifications are introduced. This permits us to write down analytic expressions for the two- and three-pulse 2D-ESR experiments described herein, which include detailed aspects of the spin relaxation.

A. Two-pulse experiment—SECSY

The two-pulse SECSY experiment [cf. Fig. 1(a)] yields three types of signals—transverse, axial, and the echo or SECSY signal. The latter provides the nuclear modulation effects. Since each term shows distinctive dependence on the phases of the pulses as shown by GF, one may cancel the transverse and axial terms by phase cycling, leaving just the SECSY signal.

The SECSY signal is

$$S_{\mathrm{SECSY}}\propto -ie^{i(2\phi_2-\phi_1)}\exp[-(2t_1+t_2)/T_{2e}]$$

$$\times\left(k_+\bar{A}+k_-F+(k/4)\sum_{i=1}^{6}M_i\right), \tag{5}$$

$$\bar{A}=\cos(\omega_+t_2),\quad F=\cos(\omega_-t_2),\quad M_1=\cos(\omega_\alpha t_1+\omega_-t_2),$$

$$M_2=\cos(\omega_\beta t_1-\omega_-t_2),\quad M_3=\cos(\omega_\alpha t_1+\omega_+t_2),$$

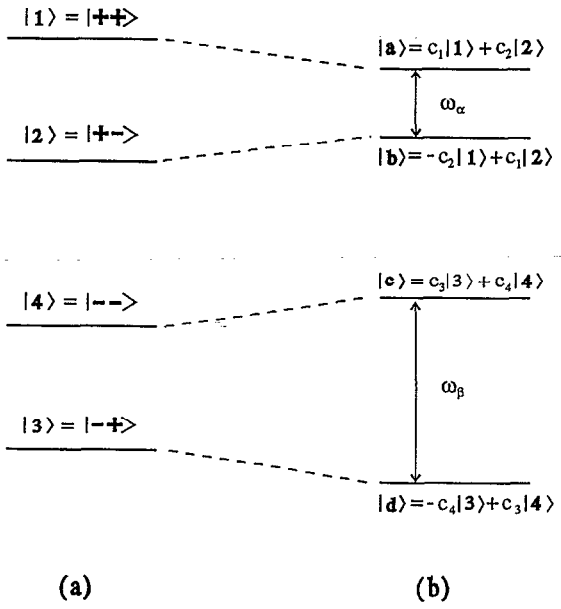

FIG. 3. The labeling of the spin eigenstates in the case of $|A/2|>|\omega_n|$. (a) The spin eigenstates in the $|S_zI_z\rangle$ basis. The first and second signs represent M_S and M_I, respectively. These spin states are eigenstates in the case of $B=0$, i.e., no pseudosecular term [cf. Eq. (3)]. (b) The spin eigenstates in the presence of the pseudosecular term. Each state can be represented as a linear combination of the basis functions in the $|S_zI_z\rangle$ basis. These eigenstates generate the $\mathscr{H}_0$ basis.

$$M_4=\cos(\omega_\beta t_1+\omega_+t_2),$$

$$M_5=-\cos(2\omega_+t_1+\omega_+t_2),\quad M_6=-\cos(2\omega_-t_1+\omega_-t_2),$$

and T_{2e} is the T_2 for electron-spin transitions. Also ϕ_1 and ϕ_2 are the phases of pulses 1 and 2.

The parameters k, k_+, and k_- appear in Table III in terms of the key frequencies ω_α and ω_β (cf. Fig. 3)

$$\omega_\alpha=\left[\left(\frac{A}{2}-\omega_n\right)^2+\left|\frac{B}{2}\right|^2\right]^{1/2},$$

$$\omega_\beta=\left[\left(\frac{A}{2}+\omega_n\right)^2+\left|\frac{B}{2}\right|^2\right]^{1/2}$$

with $\omega_\pm=\frac{1}{2}(\omega_\alpha\pm\omega_\beta)$. Note that in Eq. (5), the symbol $\bar{A}$ stands for the two allowed ESR resonances (i.e., allowed autopeaks obtained by rewriting the cosine as the sum of two exponentials), F stands for the two forbidden ESR resonances (i.e., forbidden autopeaks), and M_i ($i=1,\ldots,6$) for the 12 nuclear modulation (or coherence cross) peaks. The SECSY spectrum can be obtained by Fourier transforming Eq. (5) along both t_1 and t_2. A schematic diagram for the SECSY experiment is shown in Fig. 4(a) for the case of $|A/2|>|\omega_n|$ which is always the case regardless of the orientation angle in the γ-irradiated malonic acid single crystal. The case for $|A/2|<|\omega_n|$ can be obtained from this by swapping ω_+ and ω_- and by changing the sign of ω_β (cf. Table III). Figure 4 illustrates the rich array of modulation peaks in a manner reminiscent of NMR COSY and SECSY involving spin–spin coupling. Note that Eq.

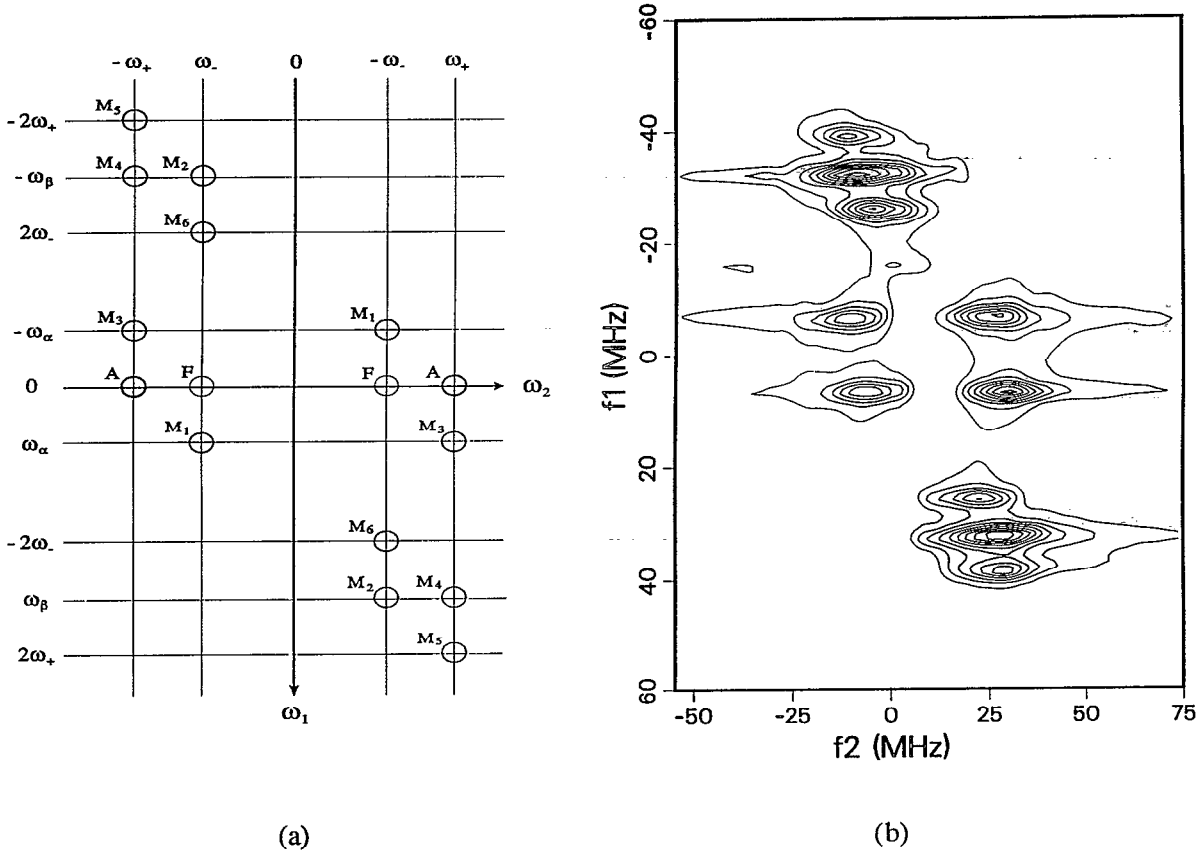

FIG. 4. (a) A schematic spectral diagram for the SECSY experiment; (b) experimental contour plot for the (30°,0°) orientation [cf. Fig. 8(b)], where the intense allowed peaks along $\omega_1=2\pi f_1=0$ have been removed.

(5) is exactly the equation previously obtained by GF, since relaxation appears in a very simple fashion in this two-pulse experiment, viz. all lines are broadened by the homogeneous T_{2e}.

In a real experiment, there is inhomogeneous broadening along the ω_2 axis, but the refocusing with respect to t_1 in the echo experiment cancels out the inhomogeneous broadening along the ω_1 axis. Therefore one can obtain T_{2e} across the whole spectrum in a 2D-SECSY experiment. The Gaussian inhomogeneous broadening effect along ω_2 is included in our simulations as follows:

$$f_b(t_2)=f(t_2)\frac{1}{\sqrt{2\pi}\Delta}\int_{-\infty}^{\infty}\exp\left(-\frac{\nu^2}{2\Delta^2}\right)e^{-i2\pi\nu t_2}\,d\nu$$

$$=f(t_2)e^{-2(\pi\Delta t_2)^2}, \qquad (6)$$

where $f_b(t_2)$ is the broadened signal and Δ is the Gaussian inhomogeneous broadening parameter in frequency units. Note that in the conversion of the internal angles (θ,ϕ) to the Euler angles, we get $(\alpha,\beta,\gamma)=(0°,-\theta,0°)$ for the zx quadrant ($\phi=0$; i.e., the rotation axis for the goniometer is parallel to the y axis); $(\alpha,\beta,\gamma)=(0°,\theta,90°)$ for zy quadrant and $(\alpha,\beta,\gamma)=(0°,90°,180°-\phi)$ for the xy quadrant. The intensity of the modulation peaks relative to the autopeaks is proportional to $k/(4k_+)$. This is plotted as a function of (θ,ϕ) and (A_{xx},A_{yy},A_{zz}) in Figs. 5 and 6. It is found that

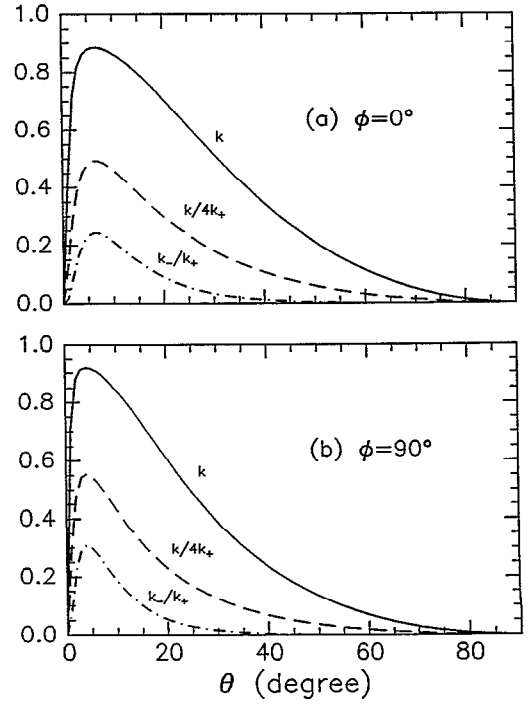

FIG. 5. The predicted variation of the intensity factors as a function of the orientation angle θ in the plane of (a) $\phi=0°$; (b) $\phi=90°$. $A_{xx}=-61$ MHz, $A_{yy}=-91$ MHz, and $A_{zz}=-29$ MHz are used.

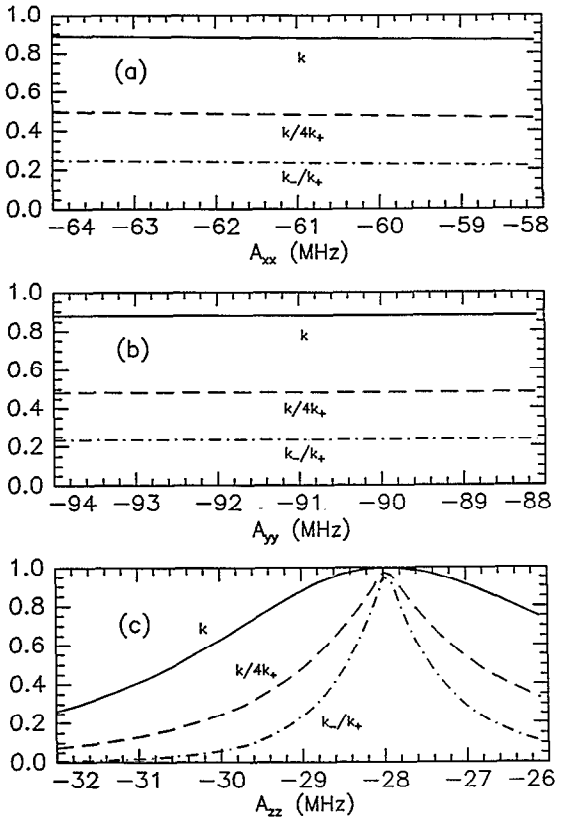

FIG. 6. The predicted variation of the intensity factors for $\theta=5°$, $\phi=0°$ as a function of the hf value (a) A_{xx}; (b) A_{yy}; (c) A_{zz}. For the fixed hf constants, $A_{xx}=-61$ MHz, $A_{yy}=-91$ MHz, and $A_{zz}=-29$ MHz are used.

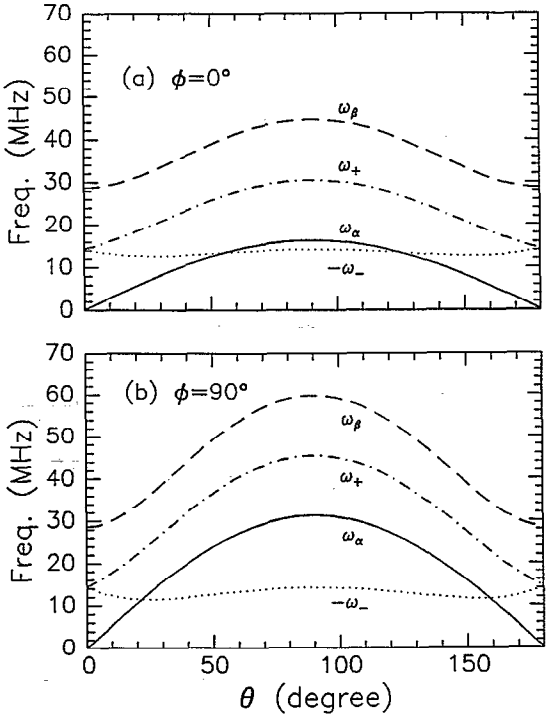

FIG. 7. The predicted angular variation of the modulation frequencies in the plane of (a) $\phi=0°$; (b) $\phi=90°$. $A_{xx}=-61$ MHz, $A_{yy}=-91$ MHz, and $A_{zz}=-29$ MHz are used.

the intensity is quite sensitive to the A_{zz} value over the range $0°<\theta<\sim 15°$. If the crystal can be mounted accurately (possibly with the help of x-ray crystallography), (A_{xx},A_{yy},A_{zz}) could be determined precisely from the intensity ratio. The modulation frequencies also show angular variation and are plotted in Fig. 7. They do not show much variation when the hf constants vary.

Simulated spectra based on the theory are shown in Fig. 8 for the zx quadrant and in Fig. 9 for the zy quadrant. As discussed in Sec. IV, where these predictions are compared with the experimental spectra, the agreement is quite good over all the orientation angles.

B. Three-pulse experiments—echo-ELDOR and stimulated SECSY

In the three-pulse experiment (cf. Fig. 1), there are, in general, nine terms—four FID-like and five echoes.[23] The relevant signal in stimulated-SECSY or 2D-ELDOR is the stimulated echo signal. The phase cycling given in Table 4 of Ref. 23 removes all the transverse and axial peaks. The S_{c-} combination of the dual quadrature signal then removes any residual FID ELDOR signal. Thus, only the stimulated echo signal is retained. The analysis based upon Appendix A yields

$$S_{\mathrm{ELDOR}} \propto -i\exp[i(\phi_3+\phi_2-\phi_1)]\exp[-(2t_1+t_2)/T_{2e}]\Big(k_+\bar{A}\{\exp[-(2W_e+2W_x)T]+\exp[-(2W_e+2W_n+\omega_{\mathrm{HE}})T]\}+k_+E\bar{A}\{\exp[-(2W_e+2W_x)T]-\exp[-(2W_e+2W_n+\omega_{\mathrm{HE}})T]\}+k_-F\{\exp[-(2W_e+2W_x)T]+\exp[-(2W_n+2W_x)T]\}+k_-EF\{\exp[-(2W_e+2W_x)T]-\exp[-(2W_n+2W_x)T]\}+\frac{k}{4}\exp[-(2W_e+2W_x)T]\sum_{i=1}^{4}M_i+\frac{k}{4}e^{-T/T_{2n}}\sum_{j=5}^{12}N_j\Big), \tag{7}$$

where

$$\bar{A}=\cos(\omega_+t_2),\quad E\bar{A}=\cos(2\omega_+t_1+\omega_+t_2),\quad F=\cos(\omega_-t_2),\quad EF=\cos(2\omega_-t_1+\omega_-t_2),\quad M_1=\cos(\omega_\alpha t_1+\omega_-t_2),$$

$$M_2=\cos(\omega_\beta t_1-\omega_-t_2),\quad M_3=\cos(\omega_\alpha t_1+\omega_+t_2),\quad M_4=\cos(\omega_\beta t_1+\omega_+t_2),\quad N_5=\cos(\omega_\alpha t_1+\omega_\alpha T+\omega_-t_2),$$

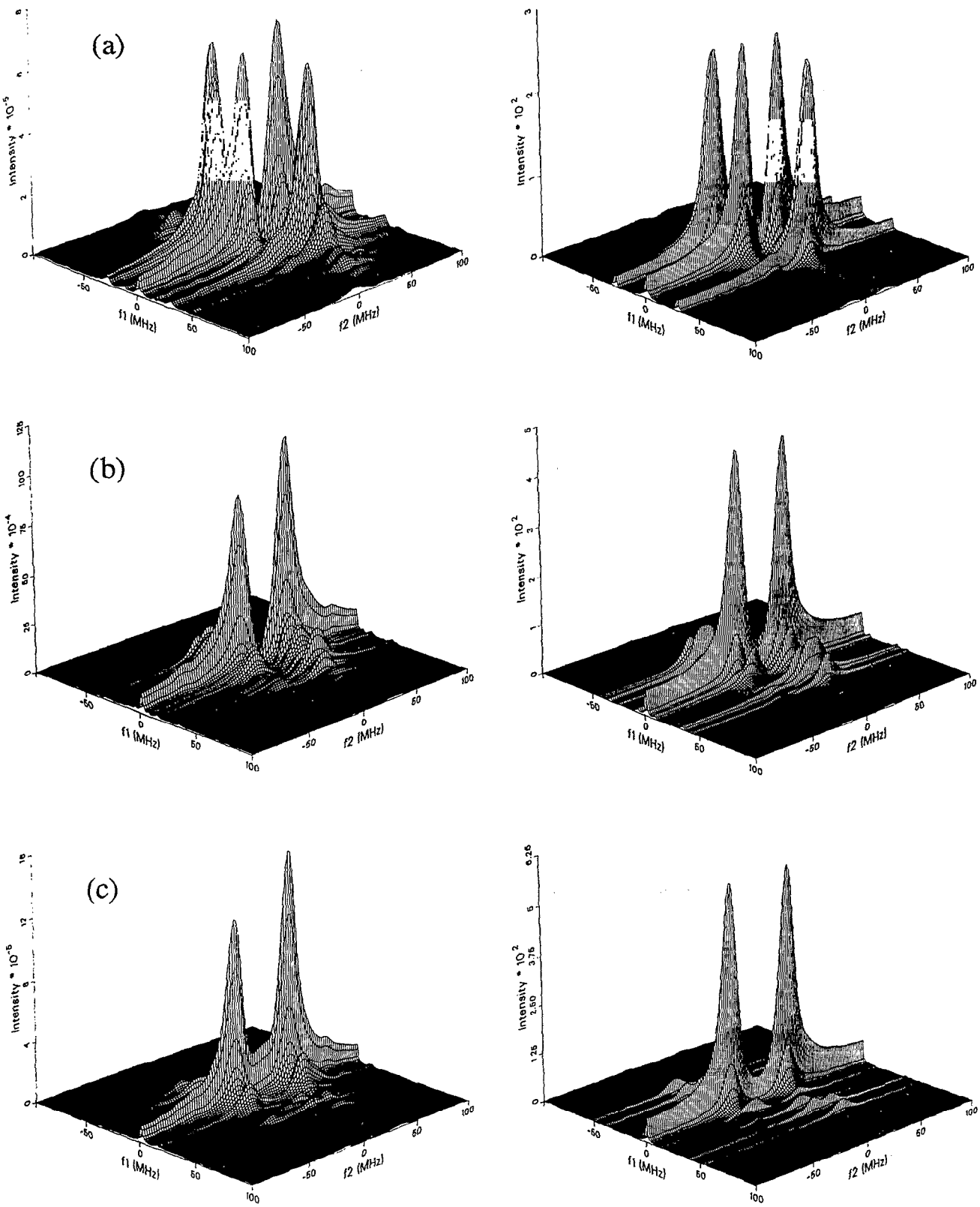

FIG. 8. Examples of experimental (left) and simulated (right) SECSY spectra at orientations of (a) (5°,0°); (b) (30°,0°); (c) (50°,0°). The measured T_2 values in Table I and the inhomogeneous broadening width $\Delta=4$ MHz are used in the simulation for each orientation.

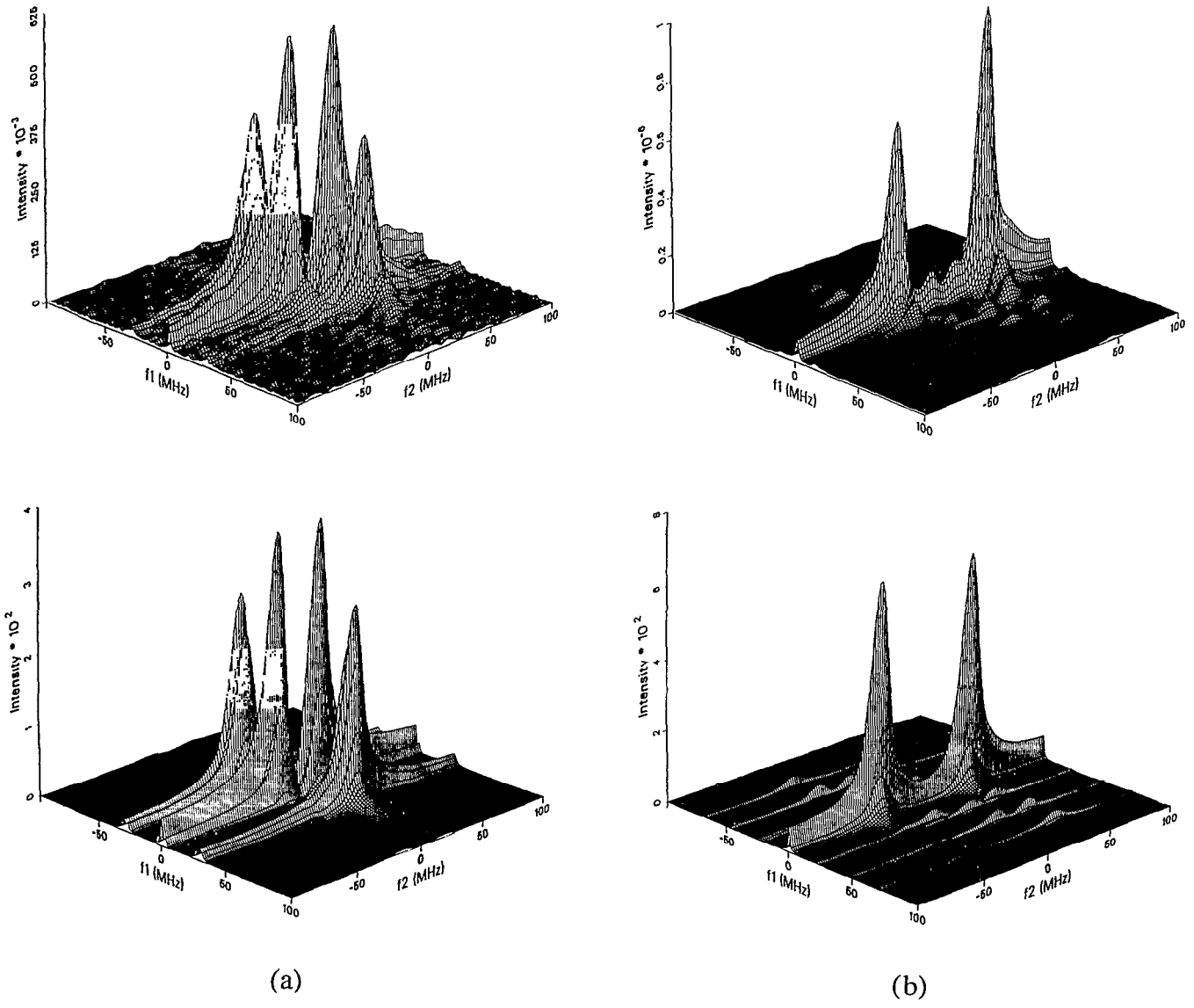

FIG. 9. Examples of experimental (upper) and simulated (lower) SECSY spectra at orientations of (a) (5°,90°); (b) (45°,90°). The measured T_2 values in Table I and the inhomogeneous broadening width $\Delta=4$ MHz are used in the simulation for each orientation.

$$N_6=\cos(\omega_\beta t_1+\omega_\beta T-\omega_- t_2),$$

$$N_7=\cos(\omega_\alpha t_1+\omega_\alpha T+\omega_+ t_2),$$

$$N_8=\cos(\omega_\beta t_1+\omega_\beta T+\omega_+ t_2),$$

$$N_9=-\cos(2\omega_- t_1+\omega_\alpha T+\omega_- t_2),$$

$$N_{10}=-\cos(2\omega_- t_1-\omega_\beta T+\omega_- t_2),$$

$$N_{11}=-\cos(2\omega_+ t_1+\omega_\alpha T+\omega_+ t_2),$$

$$N_{12}=-\cos(2\omega_+ t_1+\omega_\beta T+\omega_+ t_2),$$

and T_{2n} is the T_2 for nuclear spin transitions. Also W_e and W_n are the lattice induced electron-spin flip and nuclear spin flip relaxation rates, with W_x a measure of the cross relaxation (cf. Ref. 11 and Appendix A); ω_{HE} is the Heisenberg spin exchange[11,36] frequency (cf. Appendix A).

Equation (7) has the same allowed and forbidden autopeaks as the two-pulse SECSY expression of Eq. (5), but now there are exchange cross peaks labeled as $E\bar{A}$ and EF which show up in the 2D-ELDOR experiment. Note that only the allowed autopeaks ($\bar{A}$) and the allowed exchange peaks ($E\bar{A}$) appear to be directly relaxed by the Heisenberg exchange process in the approximations made in Appendix A (which is not a general result). However, T_{2e} and T_{2n} both have contributions from ω_{HE}.[11,36] There are two types of nuclear modulation cross peaks labeled M_i ($i=1,...,4$) and N_j ($j=5,...,12$). The M_i peaks come from spins along the z axis during the mixing period T, whereas for the N_j peaks, the spins are in the xy plane during this period, so they exhibit nuclear modulation with respect to T. In the limit of $T=0$, Eqs. (5) and (7) do become identical.

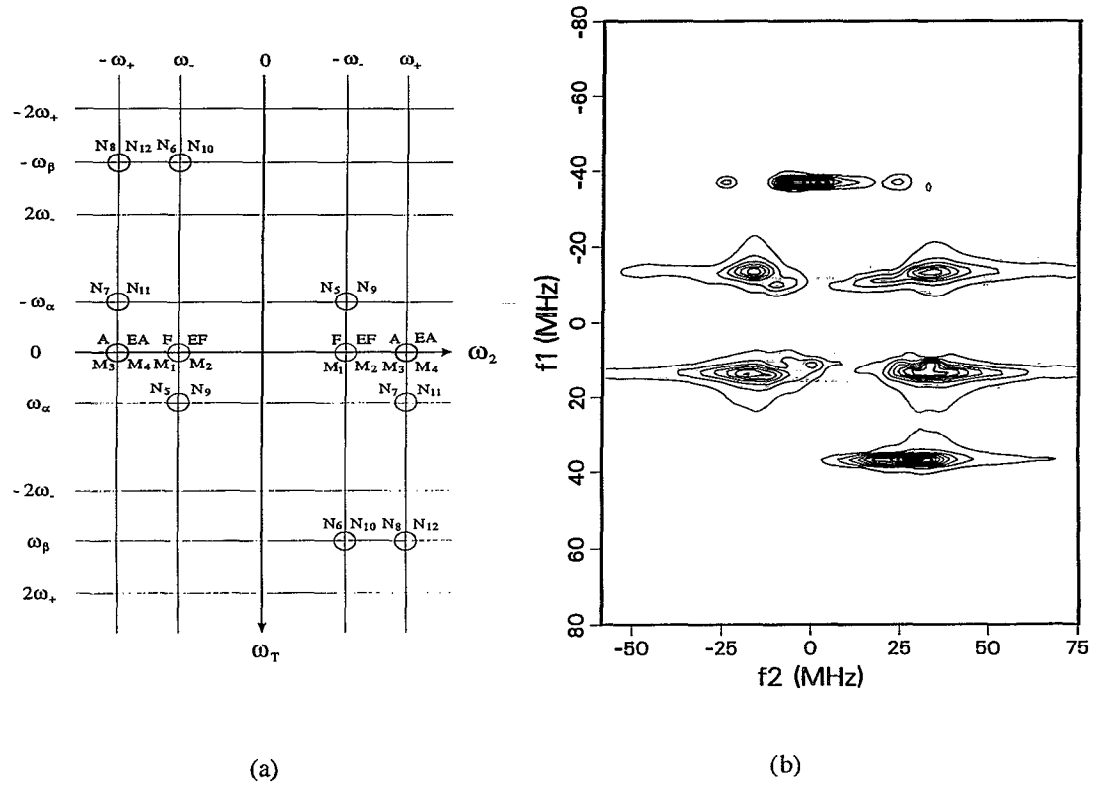

FIG. 10. (a) A schematic spectral diagram for stimulated SECSY; (b) experimental contour plot for the (50°,0°) orientation [cf. Fig. 11(b)].

Note also the more complex relaxation than given by GF. The $\bar{A}$ and F autopeaks each relax during the mixing period (i.e., vs T) as the sum of two of the three normal relaxation modes found in Appendix A, whereas the exchange cross peaks $E\bar{A}$ and EF relax according to differences in these modes. The M_i modulation peaks relax (vs T) according to one of these modes, whereas the N_j peaks relax (vs T) by T_{2n} since they are associated with nuclear transition terms during the mixing period. The GF theory[23] and its application by Patyal *et al.*[27] could not include such details of relaxation nor the exchange cross peaks. In order to get Eq. (7) to reduce to those of Refs. 23 and 27, one must let $\omega_{HE}=W_n=W_x=0$, $T_1=1/2W_e$, and $T_2=T_{2e}=T_{2n}$, which represent oversimplifications of the relaxation (cf. Appendix B).

1. Stimulated SECSY

Fourier transformation of Eq. (7) along T and t_2 gives the stimulated-SECSY spectrum, whose schematic diagram is shown Fig. 10(a) for $|A/2|>|\omega_n|$. The intensity of all the peaks at $\omega_T=\pm\omega_\alpha$ becomes zero if $\omega_\beta t_1=2n\pi$ with n an integer. This is the so-called suppression effect in conventional ESEEM. This suppression effect is seen to be due to pairs of N-type modulation peaks with opposite signs appearing at the same location in the 2D spectrum (i.e., N_5 and N_9, and N_7 and N_{11}). t_1 is preset to avoid the suppression effect in the experiment. A series of simulated spectra are shown in Fig. 11. They are compared to experimental spectra (also in Fig. 11) in Sec. IV and are found to agree well over all the orientation angles.

2. Echo-ELDOR

The echo-ELDOR spectrum is obtained by Fourier transform of Eq. (7) along t_1 and t_2 and its illustrative diagram is shown in Fig. 12. The general pattern is the same as that for SECSY (cf. Fig. 4), but now there are pairs of modulation terms (but all of the same sign) contributing to the nuclear modulation cross peaks, i.e., there is no suppression effect. However, the relative intensities in 2D-ELDOR contain considerable information on the relaxation parameters. Another important difference is the existence of exchange cross peaks ($E\bar{A}$ and EF) which grow in with T due to W_n or W_x. If $W_n>W_x$, the exchange cross peaks between the allowed transitions ($E\bar{A}$) have the same sign as the autopeak. If $W_n<W_x$, they have the opposite sign. Therefore the source of the exchange cross peaks determines the phase, which can be obtained before taking the magnitude spectrum. However, the observation of $E\bar{A}$ is somewhat obscured because the nuclear modulation peaks N_{11} and N_{12} appear at the same positions and their phases do depend on T.

Simulated spectra, selected to compare with experimental ones in Fig. 13, are shown in Fig. 14. They are a good example of how the relaxation parameters can be derived from the echo-ELDOR spectra with different mixing time. It is convenient to use a relative intensity scale since the intensity of the allowed autopeak ($\bar{A}$) itself is a

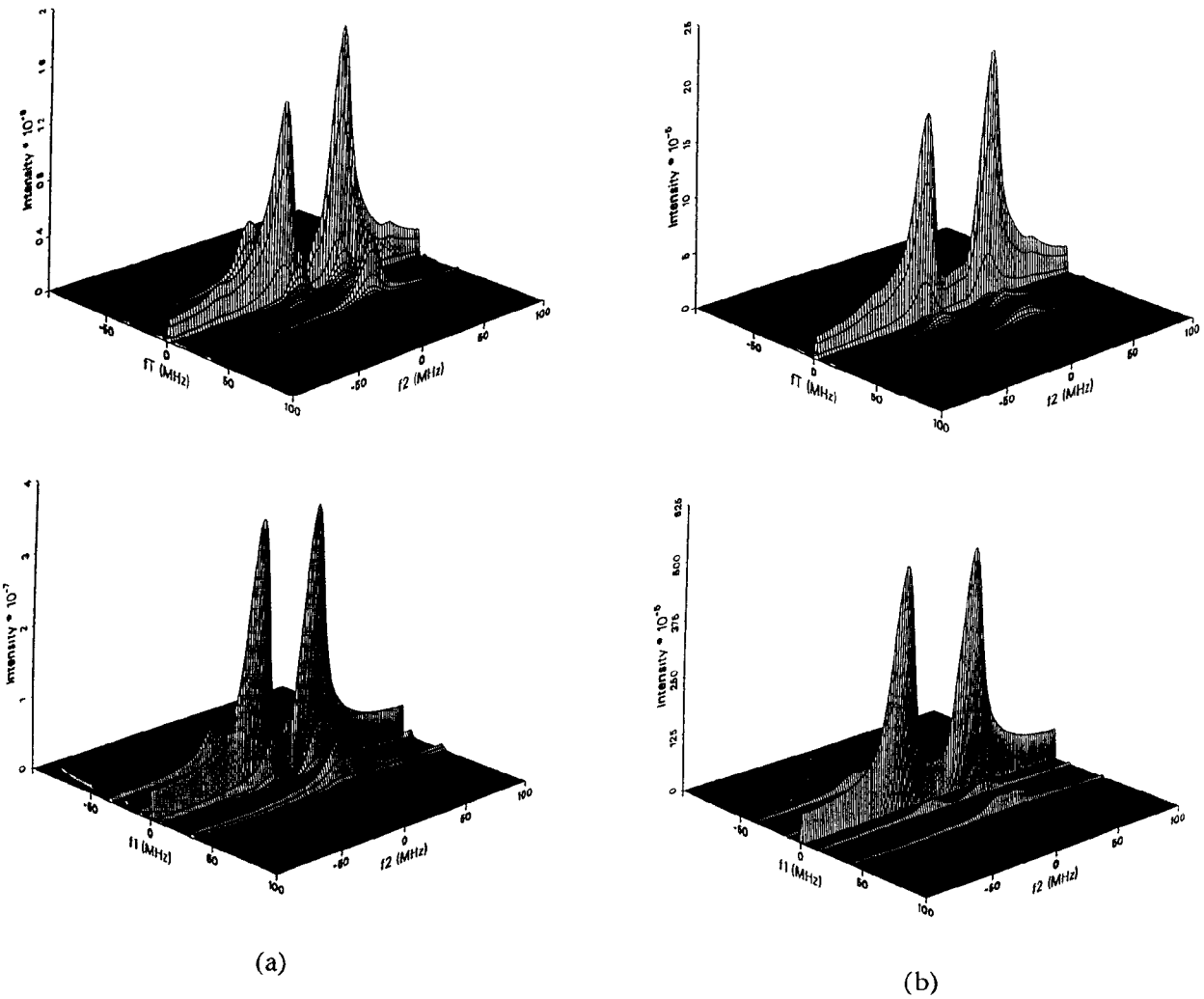

FIG. 11. Examples of experimental (upper) and simulated (lower) stimulated SECSY spectra at orientations of (a) (30°,0°); (b) (50°,0°). The parameters used in the simulation are $T_{2e}=900$ ns, $T_{2n}=22$ μs, $W_e=1.67\times10^4$ s^{-1}, $W_n=7.14\times10^3$ s^{-1}, $W_x=6.17\times10^3$ s^{-1}, and $\Delta=5$ MHz.

function of T (i.e., let the intensity of peak $\bar{A}$ be unity). The development of the exchange cross peaks ($E\bar{A}$) can be clearly seen as the mixing time T increases.

IV. RESULTS AND DISCUSSION

A. SECSY

We show in Figs. 8 and 9 a series of SECSY spectra obtained for a range of values of orientation angles θ and ϕ. These 2D spectra were obtained by a 2D-FFT of the raw experimental data. One sees that the modulation peaks vary dramatically as a function of orientation as predicted (cf. Figs. 5 and 7). The modulation peaks are a maximum for a small value of $\theta\cong5°$ (either for $\phi=0°$ or 90°) and are comparable in magnitude to the autopeaks. The complex modulation pattern predicted (cf. Fig. 4) becomes more differentiated for larger values of $\theta\sim(30°$–$50°$, $\phi=0°$ or 90°), where the intensities of the modulation peaks are significantly less than those of the autopeaks and the separation of the peaks ω_α is large. Also included for comparison are the simulated spectra appropriate for the particular orientation, the measured T_{2e} (which is found to be orientation dependent, as expected), and the observed inhomogeneous broadening. The simulations do not include contributions from secondary radical species known to be present,[30] nor the nuclear modulation from matrix protons which appear along f_1 at the nuclear Zeeman frequency $\omega_n\cong14$ MHz. The general agreement between experiment and theory is seen to be excellent with respect to the features due to the α proton of malonic acid, and they are the dominant features. In order to more clearly discern the characteristic patterns of the modulation peaks diagrammed in Fig. 4(a), we display a contour plot for one of the orientations ($\theta=30°$, $\phi=0°$) in Fig. 4(b). This contour was processed by applying LPSVD to the data of Fig. 8(b). This enabled us to remove the dominant autopeaks which would otherwise overwhelm the contour plots, as well as the broad contributions presumably from the matrix protons (at $f_1=\pm13.5$ MHz). Indeed, one discerns all the modulation peaks with the expected overlaps of

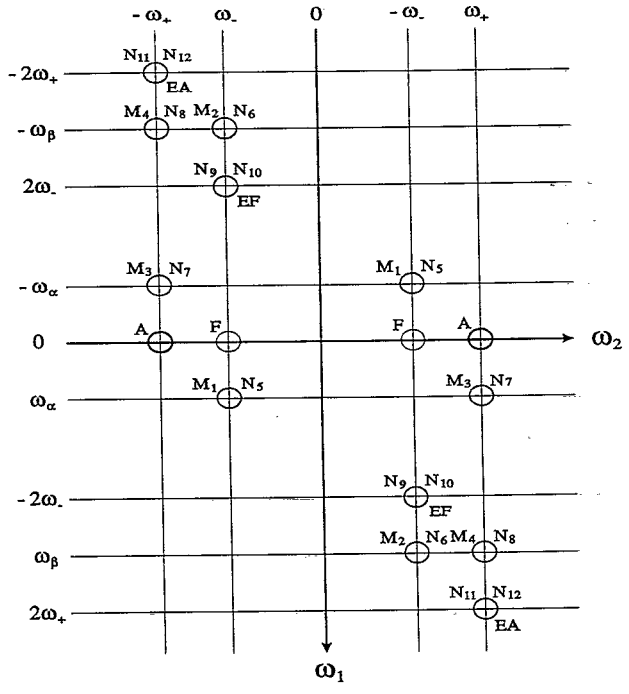

FIG. 12. A schematic spectral diagram for the echo-ELDOR experiment.

peaks that are nearby. The two pairs of M_1 and M_3 peaks are clearly distinguishable. The two groupings of the M_2, M_4, M_5, and M_6 peaks are also clearly discernible. Although overlapped, one sees the M_5 and M_6 peaks, while the M_2 and M_4 peaks, both of which occur at $\omega_1=\omega_\beta$, form a broad doubled-width line as expected since the inhomogeneous broadening affects only the ω_2 direction (and not the ω_1 direction in this echo-based experiment).

B. Stimulated SECSY

In Fig. 11, we show stimulated SECSY spectra for several orientations as well as the respective simulations. Again, the characteristic features predicted for the α proton of malonic acid are clearly discerned in the experimental spectra. We further examine the modulation patterns by first using LPSVD to remove the autopeaks along $\omega_1=0$. As can be seen from Fig. 10(a), the M_i $(i=1,...,4)$ modulation peaks are degenerate with the autopeaks and are therefore not observed. The remaining spectrum showing the N_j $(j=5,...,12)$ modulation peaks is displayed in the contour plot of Fig. 10(b) [based on the data of Fig. 11(b)] corresponding to $\theta=50°$, $\phi=0°$. One clearly discerns the two pairs of N_5+N_9 and N_7+N_{11} peaks at $\omega_T=\pm\omega_\alpha$ as well as the broadened-out groupings of N_6+N_{10} with N_8+N_{12}. Because of the suppression effect in stimulated SECSY, the intensities for each grouping are influenced differently for the particular value of t_1 one utilizes (see below), and this influences somewhat the pattern seen in the contour plot.

The LPSVD data analysis of the spectra with 250 ns T step size show that we have only a single exponential decay along the T axis for the allowed autopeaks $(\bar{A})$, whereas the theory predicts the superposition of two distinctive decays $1/(2W_e+2W_x)$ and $1/(2W_e+2W_n)$ within our relaxation scheme; (we assume $\omega_{\rm HE}\cong 0$, i.e., our crystal is dilute enough to neglect concentration-dependent spin relaxation processes). This might be due to the fact that those two decays are very close and LPSVD cannot distinguish their difference. However, Eq. (7) shows stimulated-SECSY gives direct information on the normal modes of relaxation which cannot in general be ascribed to a simple T_{1e}.

C. 2D-ELDOR

We show in Fig. 13 a sequence of 2D-ELDOR experiments for a particular orientation ($\theta=30°$, $\phi=0°$). First of all, we wish to comment that the 2D-ELDOR spectra due to the nuclear modulation are very similar to the SECSY spectrum for the same angle, although differences in intensity do arise from the different dependences on T of the various modulation peaks and their different relaxation dependences [cf. Eq. (7)]. In general, we do observe that the 2D-ELDOR spectra are similar to the SECSY spectrum for the equivalent crystal orientation. Thus, we only display in Fig. 13 spectra for a single orientation, but as a function of the mixing time, T. We display in Fig. 14 a set of simulations of the 2D-ELDOR experiment for the range of mixing times, and again generally good agreement between theory and experiment is observed. The changes with T are seen to be rather subtle. We can perhaps observe them more clearly in the contour plot format wherein the dominant autopeaks along $\omega_1=0$ are removed by LPSVD. A series of contours are shown in Fig. 15. These do indeed display the basic SECSY pattern seen in Fig. 4. As one looks with greater detail, one observes some significant variations with T. The intensity of the forbidden peaks is much smaller than that of the allowed peaks $(k_-/k_+\cong 0.03)$ for this orientation (cf. Fig. 5). Therefore we can ignore the contribution of F and EF. The modulation frequency ω_β from the experimental spectra is ~ 32 MHz, which implies the actual orientation is approximately (25°,0°). The frequency ω_α is a little obscured by the broadening effect of the autopeaks. Once each term in Eq. (7) is classified according to the position of the peak by the following equation and its equivalents:

$$\cos(2\omega_- t_1+\omega_\alpha T+\omega_- t_2)$$
$$=\tfrac{1}{2}e^{i\omega_\alpha T}\exp[i(2\omega_- t_1+\omega_- t_2)]+\tfrac{1}{2}e^{-i\omega_\alpha T}$$
$$\times\exp[-i(2\omega_- t_1+\omega_- t_2)] \qquad (8)$$

the calculation of the absolute intensities at each peak position including the relaxation constants shows

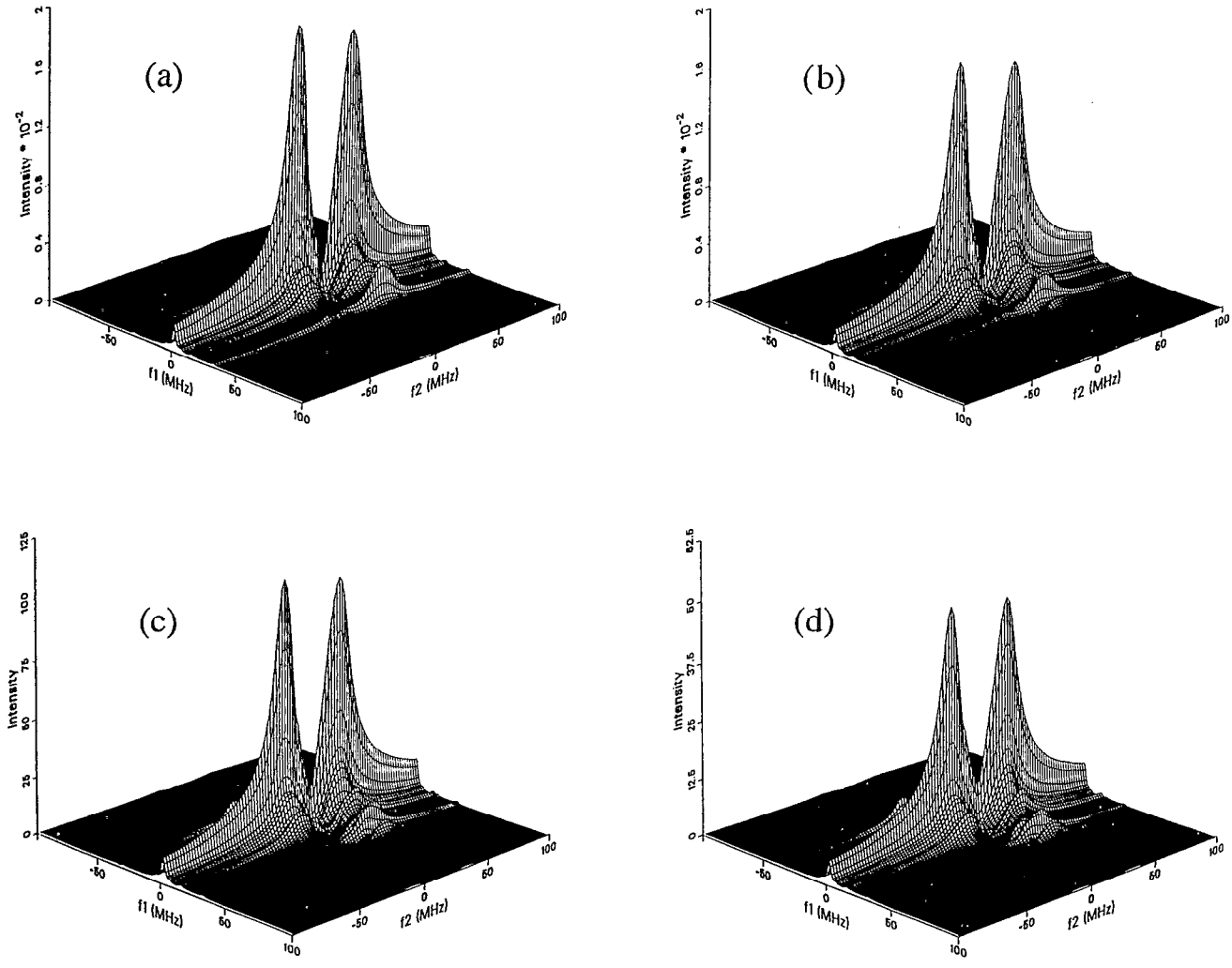

FIG. 13. Stacked plots of the experimental echo-ELDOR spectra at the orientation of (30°,0°) with mixing time (a) $T=5$; (b) 20; (c) 40; (d) 60 μs.

$$M_1+N_5 \text{ or } M_3+N_7 \text{ depends on } \frac{k}{4}\{\exp[-(2W_e+2W_x)T]+e^{-T/T_{2n}}e^{i\omega_\alpha T}\},$$

$$M_2+N_6 \text{ or } M_4+N_8 \text{ depends on } \frac{k}{4}\{\exp[-(2W_e+2W_x)T]+e^{-T/T_{2n}}e^{i\omega_\beta T}\}, \tag{9}$$

$$N_9+N_{10} \text{ depends on} -\frac{k}{8}e^{-T/T_{2n}}(e^{i\omega_\alpha T}+e^{-i\omega_\beta T}),$$

$$N_{11}+N_{12}+E\bar{A} \text{ depends on} -\frac{k}{8}e^{-T/T_{2n}}(e^{i\omega_\alpha T}+e^{i\omega_\beta T})+k_+\{\exp[-(2W_e+2W_x)T]-\exp[-(2W_e+2W_n)T]\}.$$

The intensity of the N_9+N_{10} pair can be different from that of the $N_{11}+N_{12}$ pair due to their different phase dependence with respect to T in the ELDOR experiment. Note that for $T=5$ μs, the $N_{11}+N_{12}$ pair, which is degenerate with the allowed exchange cross peak ($E\bar{A}$) appears to be missing. Such an effect is due likely to the opposite phase of $N_{11}+N_{12}$ with $E\bar{A}$. As T increases, one observes that this (composite) peak grows in relative to the others, so that by $T=60$ μs, it has become a dominant feature. This can only be explained by the growing in of the exchange peak relative to the modulation peaks as predicted by Eq. (7) provided there is a substantial W_n or W_x.

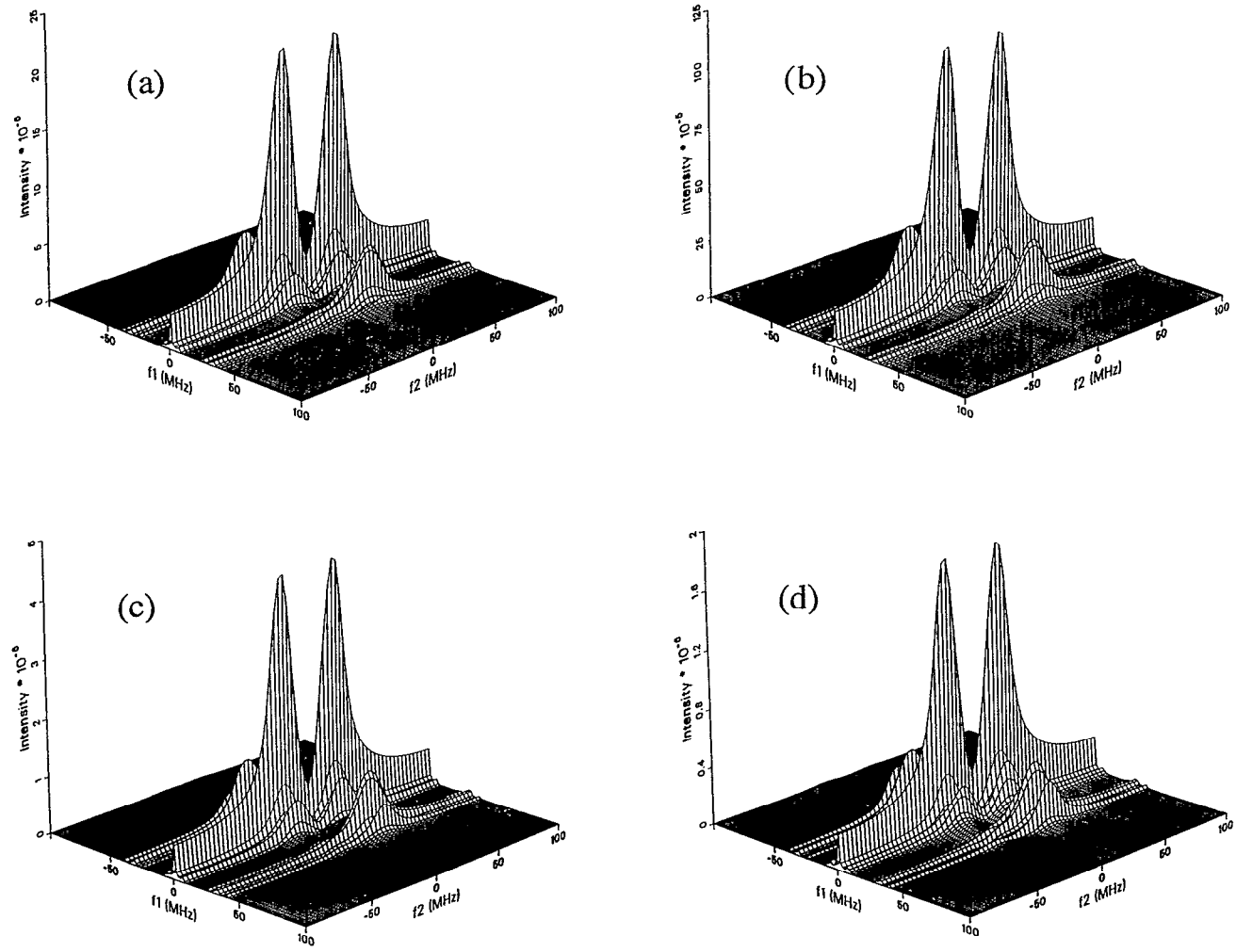

FIG. 14. The simulated echo-ELDOR spectra corresponding to Fig. 13. The same parameters as in Fig. 11 are used.

Note that the phases of the complex number quantities $e^{i\omega T}$ are rapidly oscillating. For $\omega_\beta=32$ MHz, $e^{i\omega_\beta T}$ oscillates 32 cycles over a 1 μs period. This shows the intensity of the N_j peaks would be oscillating. When the intensity of the M_i terms and the exchange term is comparable to that of N_j terms, the intensity of the peaks where M_i+N_j and $N_{11}+N_{12}+E\bar{A}$ terms appear would also be rapidly oscillating. It is thus very difficult to obtain the phase of each peak with only five different mixing times since the intensity is a function of the relaxation constants and the modulation frequencies. Therefore, a slight uncertainty in the modulation frequencies from the value of the magnetic constants and the orientation of the single crystal leads to substantial uncertainty in the determination of the relaxation constants. Thus it is first important to measure the modulation frequencies accurately (and to accurately orient the single crystal) prior to analyzing the spin relaxation. Then a series of experiments with many mixing times stepped by $\sim$200 ns, so that the contribution of the exchange peak is almost constant over several steps, would be useful to determine the phase of the peaks more accurately, since the modulation frequencies ω_α and ω_β are about 7 and 32 MHz, respectively.

Even though the present work was not performed in this fashion, we were able to utilize our LPSVD data analysis as well as measurements of the peak heights to constrain our choices of relaxation parameters, according to the following observations:

(i) The existence of exchange cross peaks is clearly indicated by the following: The peaks at $(\omega_1,\omega_2)=(\pm 2\omega_+,\pm\omega_+)$ given by an $(N_{11}+N_{12}+E\bar{A})$ increase with T, for $T>20$ μs, relative to the $\bar{A}$ peaks. [Note that the (N_9+N_{10}) peaks do not show much variation relative to the $\bar{A}$ peaks.]

(ii) At no time for $T\leqslant 60$ μs do the $E\bar{A}$ peaks become dominant over the $(N_{11}+N_{12})$ peaks. Given the variation in phase of these latter peaks with T [cf. Eq. (9)] and other instrumental contributions to the phase of the various

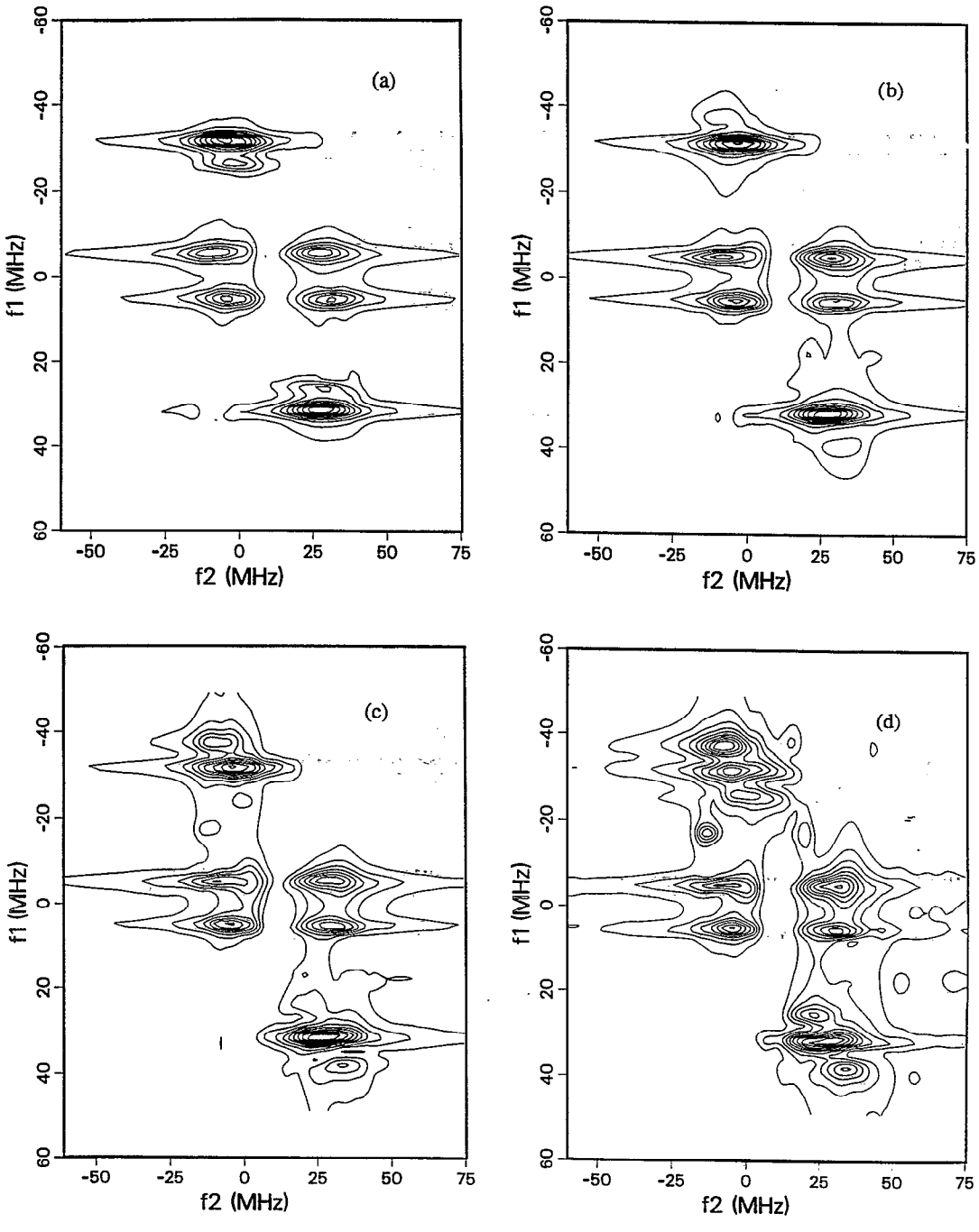

FIG. 15. Contour plots of the echo-ELDOR spectra shown in Fig. 13.

peaks,[26] we could not reliably determine the sign of $E\bar{A}$ relative to $\bar{A}$.

(iii) However, we do observe that the relative intensity of the exchange peak (i.e., $|E\bar{A}/\bar{A}|$) grows to $\sim$0.06–0.10 in $T=60$ μs. Since $|E\bar{A}/\bar{A}|=[1-\exp(-|2W_n-2W_x|T)]/[1-\exp(-|2W_n-2W_x|T)]$, then we roughly estimate $|2W_n-2W_x|\sim 2\text{–}3\times 10^3$ s^{-1}.

(iv) The stimulated SECSY experiment yielded a decay constant of 21.1 μs which should be close to the similar values of $1/(2W_e+2W_x)$ and $1/(2W_e+2W_n)$.

The T_2's were constrained by

(v) the SECSY experiment yielding $T_{2e}=900$ ns;

(vi) the ratio of the peaks (N_9+N_{10}) vs (M_2+N_6) grows with increasing T, corresponding to the M vs N peak ratio decreasing with T. This yields $T_{2n}^{-1}<(2W_e+2W_x)$, but the relation $T_{2n}^{-1}=T_{2n}'^{-1}+W_e+W_n+W_x$ [cf. Eq. (B2)] yields $T_{2n}^{-1}>W_e+W_n+W_x$. These two inequalities provide bounds for T_{2n}^{-1}.

TABLE II. T_2 variation of the main peaks for different mixing time.

Orientation	Mixing time (μs)	Average T_2 of the two main peaks (ns)					
		0[a]	5	20	30	40	60
(30°,0°)		908	763	588	549	503	445
(50°,0°)		928	718	452	439	402	317

[a]T_2 for zero mixing time is obtained from the SECSY experiment.
[b]All the experiments are performed with 5 ns t_1 step size.

The parameters were varied within these constraints to fit the set of 2D-ELDOR spectra for different T. This enabled us to obtain W_e more precisely and from that estimates of the absolute values of W_x and W_n, as well as T_{2n}^{-1}. We arbitrarily chose $W_n > W_x$ (but we could fit the 2D spectra equally well with $W_x > W_n$). These results are given in the caption to Fig. 11.

D. 2D-ELDOR "motional" cross peaks

Patyal *et al.*[27] showed in their study of a nitroxide in a glycerol host that the 2D-ELDOR main peaks broaden with mixing time T. This is consistent with the development of "rotational cross peaks" as the molecule slowly reorients during the mixing time. That is, one is observing how the slow motions evolve in real time.

We have examined the time evolution of the apparent widths of the main peaks as a function of T for several crystal orientations. Indeed we do find a broadening as T increases which we can ascribe to some slow dynamical process in the single crystal. {Note that we use the fact that 2D-ELDOR at $T=0$ is exactly the same as the SECSY-ESR experiment [cf. Eqs. (5) and (7)] to obtain the former.} We provide these results in Table II. Note that the modulation peaks are, in general, observed to broaden with T (cf. Fig. 15), but because of their lower intensity and overlap effects, our analysis of them proved less accurate. We find over the 60 μs period that the intrinsic T_2 of 908 ns broadens in the 2D-ELDOR experiment to 445 ns for the orientation of ($\theta=30°$, $\phi=0°$). This corresponds to an increase in "width" of about 0.34 MHz. The same analysis for ($\theta=50°$, $\phi=0°$) leads to a 0.26 MHz increase. This is to be compared with the inhomogeneously broadened hf width along ω_2 of about 4–5 MHz.

In speculating about the nature of the processes being observed, we wish to note that there are two classes of dynamic processes which could have the correct qualitative behavior. First are the solid-state "spin-dynamics" processes related to spectral diffusion, in particular, spin diffusion of the proton spins[37–39] in the malonic acid crystal. The weak dipolar coupling of the unpaired electron spin of the malonic acid radical with surrounding matrix protons will lead to a distribution of local frequency shifts that would contribute to the inhomogeneous broadening of the cw ESR line. However, spin diffusion within the manifold of matrix protons will modulate these local frequency shifts in a time-dependent fashion. If this modulation were not too fast, then this phenomenon could lead to a broadening of the 2D-ELDOR peaks as T increases, i.e., a spectral diffusion. However, Mims[37] has argued that one should be in the "narrowing" regime, since estimates of the frequency shifts caused by the nuclear spin diffusion are small compared to the rate of nuclear spin flip flops, which are the basis of the spin-diffusion process. Such "motional averaging" would contribute to the homogeneous T_{2e},[37,38] but would not contribute to the broadening of the 2D-ELDOR peaks vs T. But the detailed mechanism is a complex one, and more careful analyses suggest otherwise,[37,39] since the nuclear-spin flip–flop times (estimated as $\sim 10^{-3}$–10^{-4} s) are long compared to the time scale of the experiment. As formulated for experiments at low temperatures (77 K or lower[38,39]), this spectral diffusion process is temperature independent, but at room temperature, one might anticipate a thermal enhancement of nuclear spin flip–flop rates.

At higher electron spin concentrations, there are equivalent spectral diffusion processes whereby nearby electron spins cause local frequency shifts of each electron spin, and these frequency shifts are modulated either by electron-spin diffusion within the electron-spin manifold ("T_2-type samples"), or by T_{1e} processes ("T_1-type samples").[38,39] In T_2-type samples, mutual flip flops of electron spins can also be effective,[38,39] as outlined in Appendix A. These and related electron-spin–spin processes have been studied in malonic acid by electron-spin echoes at low (77 K) temperatures.[40] There are, however, subtle distinctions which affect the role of such processes in our present 2D experiments with nonselective microwave pulses that irradiate the whole ESR spectrum.[41]

At room temperature, where thermally activated processes become more important, we may expect a second class of processes to contribute to the observed broadening of the 2D-ELDOR peaks with respect to T. In particular, phonon modes may be expected to modulate the amplitude and orientation of the malonic acid proton hf and g tensors[42] which dominate the spin Hamiltonian. This would lead to the relaxation effects outlined in the appendices. However, those phonon modes that are at the low frequency end of the phonon spectrum could induce slow fluctuations in the hf and g tensors, which can lead to spectral diffusion that broadens the 2D-ELDOR main peaks as a function of mixing time T. Let us, for the moment, suppose that the dominant phonon modulation is orientational, i.e., there is a slow phonon-induced torsional oscillation in the crystal. We find from Fig. 7(a) that for ($\theta=30°$, $\phi=0°$), a change of 0.3 MHz in resonant frequency ω_+ would correspond to an angular change of about 1.3°, consistent with a small oscillation. (We get a 1.2° change for $\theta=50°$, $\phi=0°$.)

We expect that further studies, especially as a function of temperature, would be helpful to clarify the source of the 2D-ELDOR "motional" cross peaks. We do, however, wish to note that in a preliminary 2D-ELDOR study of a nitroxide spin-labeled organic polymer in a polycrystalline state at room temperature, *no change* was observed in the 2D-ELDOR peaks with mixing time T.[43] The mechanism

of spin diffusion of the matrix protons should be quite general (except perhaps to the extent to which it is motionally narrowed), whereas phonon modulation should be specific to the medium. Clearly, also the larger concentrations of spins in the malonic acid case could imply contributions from electron-spin–spin interactions mentioned above.

In either case, by observing the real time evolution in a 2D-ELDOR experiment, we observe how each malonic acid radical samples the range of local sites available to it as a result of the slow dynamics. We further note that, whereas the measured T_1's and T_2's reflect the effects of crystal dynamic modes that are usually fast on the ESR time scale, the 2D-ELDOR "motional" cross peaks are manifestations of the processes that are slow on the ESR time scale.

V. CONCLUSIONS

The techniques of SECSY ESR, stimulated SECSY, and 2D ELDOR have been applied successfully to a single crystal of irradiated malonic acid and generally excellent agreement with theory is obtained for the nuclear modulation patterns in all these cases.

It has been possible to combine the well-known theories for nuclear modulation in spin-echo spectroscopy and spin relaxation in a single general format in Liouville space. This analysis has confirmed the relative simplicity of two-pulse nuclear modulation experiments with regard to relaxation, viz. only T_{2e} is of significance. (For simplicity, in our present analysis we ignored any differences of T_{2e} for the different allowed and forbidden transitions, although such differences are included in the general theory.) However, the analysis explicitly displays the much more complex dependencies on relaxation for the three-pulse nuclear modulation experiments, wherein T_{1e}, T_{1n}, T_{2n}, and cross relaxation also play an important role, such that the main allowed peaks and two different classes of modulation peaks are affected differently. It was illustrated how this richness of relaxation behavior could be utilized to obtain all these various relaxation rates from a set of 2D-ELDOR experiments vs mixing time (which can be complemented by stimulated-SECSY experiments). Given the very simple dependence on relaxation of SECSY ESR, this simple two-pulse 2D-FT method would be the easiest to implement in a quantitative fashion for the study of structure by nuclear modulation. The enhanced resolution for structural studies obtained by SECSY ESR was previously demonstrated in frozen samples containing many weakly coupled protons and/or deuterons.[26] The present study has shown that by using very short $\pi/2$ pulses (5 ns), in conjunction with sufficiently wide bandwidth, it is possible to obtain quantitatively the nuclear modulation patterns from a strongly coupled proton.

The three-pulse 2D-ELDOR experiment leads to a modulation pattern that is very similar to that of SECSY ESR; in fact, they become equivalent for zero mixing time. Thus, whereas the characteristic suppression effect of three-pulse ESEEM is retained in stimulated SECSY, it is absent in 2D ELDOR. We have shown how by studies as a function of mixing time, exchange peaks can be discriminated from modulation peaks, although there can be oscillations in intensities of some of the modulation peaks as a function of mixing time.

Despite the fact that stimulated SECSY suffers from the suppression effect, it does yield the simplest modulation patterns of the three experiments considered in this work. This can be a virtue in studies involving many nuclei. Intensities of the main allowed peaks and the nuclear modulation peaks do depend somewhat differently on the relaxation, which shows up as homogeneous "T_2-like" effects with respect to ω_T (i.e., the mixing time dimension). It should be noted that the relative simplicity of the stimulated SECSY pattern is due in large part to the degeneracy of one class of modulation peaks with the main allowed peaks.

An interesting and potentially important observation was made in the 2D-ELDOR experiment that is characterized as the real time evolution of "motional" cross peaks. This feature should be studied in greater detail as it would allow for the direct study of dynamical processes in solids that are slow on the ESR time scale such as spin diffusion and/or slow phonon modes.

Both 2D-ELDOR and stimulated SECSY are 2D projections of a basically 3D experiment with 2D-ESEEM of Merks and de Beer the other possibility, which, however, lacks the multiplexing advantage. We would suggest that a full 3D experiment be performed by performing 2D ELDOR over a range of mixing times. Afterward, various one- and two-dimensional projections (or slices) of the full 3D experiment could be obtained as desired.

Finally, in this context, we wish to note that the basic premise of this work, viz. to employ full collection of the echo decay resulting from nonselective irradiation of the full spectrum in a FT format, can be combined with recently suggested four- and five-pulse sequences for the study of ESEEM,[44,45] thereby enhancing these pulse sequences by the multiplexing advantage of data acquisition and by the additional spectral dimension.

ACKNOWLEDGMENTS

The authors wish to thank Dr. Dan Gamliel and Dr. Richard H. Crepeau for helpful discussions. This work was supported by NSF Grant No. CHE9004552 and by NIH Grant Nos. GM25862 and RR07126.

A preliminary account of this work was presented at the 14th International EPR Symposium; Denver, CO, August 1991.

APPENDIX A: THE DENSITY MATRIX ANALYSIS FOR NUCLEAR MODULATION INCLUDING DETAILED SPIN RELAXATION

In this appendix, we first review the basic solutions for nuclear modulation of an $S=1/2$, $I=1/2$ spin system for two- and three-pulse 2D-ESR. This is carried out in the

usual way in Hilbert space. We then develop the relaxation matrix solution in Liouville space utilizing these results.

1. Transformation from the $|S_zI_z\rangle$ basis to the basis that diagonalizes the Hamiltonian in Hilbert space

[This subsection summarizes well-known results (cf. Ref. 4) in order to provide needed definitions of terms.]

The Hamiltonian for the nuclear modulation problem in the absence of the radiation field is

$$\hat{H}=CS_z-\omega_nI_z+AS_zI_z+\tfrac{1}{2}BS_zI_++\tfrac{1}{2}B^*S_zI_-. \tag{A1}$$

It can be written in matrix form as

$$\mathbf{H}=\begin{array}{c} \begin{matrix} |1\rangle=|++\rangle & |2\rangle=|+-\rangle & |3\rangle=|-+\rangle & |4\rangle=|--\rangle \end{matrix} \\ \begin{bmatrix} (C-\omega_n+A/2)/2 & B/4 & 0 & 0 \\ B^*/4 & (C+\omega_n-A/2)/2 & 0 & 0 \\ 0 & 0 & (-C-\omega_n-A/2)/2 & -B/4 \\ 0 & 0 & -B^*/4 & (-C+\omega_n+A/2)/2 \end{bmatrix} \end{array}. \tag{A2}$$

Note that by Eqs. (4) in the main text, A, B, and C are functions of the orientational angles β and γ. This Hamiltonian is diagonalized by the similarity transform $\mathbf{T}^\dagger\hat{\mathbf{H}}\mathbf{T}=\mathbf{E}$, where

$$\mathbf{T}=\begin{pmatrix} \mathbf{T}_\alpha & 0 \\ 0 & \mathbf{T}_\beta \end{pmatrix}=\begin{pmatrix} c_1 & c_2 & 0 & 0 \\ -c_2 & c_1 & 0 & 0 \\ 0 & 0 & c_3 & c_4 \\ 0 & 0 & -c_4 & c_3 \end{pmatrix},$$

$$\mathbf{E}=\begin{array}{c} \begin{matrix} |a\rangle & |b\rangle & |c\rangle & |d\rangle \end{matrix} \\ \begin{pmatrix} C/2+\omega_\alpha & 0 & 0 & 0 \\ 0 & C/2-\omega_\alpha & 0 & 0 \\ 0 & 0 & -C/2+\omega_\beta & 0 \\ 0 & 0 & 0 & -C/2-\omega_\beta \end{pmatrix} \end{array}. \tag{A3}$$

From Eq. (A3), we see that the eigenvectors $|a\rangle$ and $|b\rangle$ are linear combinations of $|1\rangle$ and $|2\rangle$, while $|c\rangle$ and $|d\rangle$ are linear combinations of $|3\rangle$ and $|4\rangle$. We shall refer to the eigenvectors $|a\rangle$, $|b\rangle$, $|c\rangle$, and $|d\rangle$ as the $\mathscr{H}_0$ basis. Also, ω_α, ω_β and the c_i's are defined as follows:

$$\begin{aligned} \omega_\alpha&=\left[\left(\frac{A}{2}-\omega_n\right)^2+\left|\frac{B}{2}\right|^2\right]^{1/2}, \\ \omega_\beta&=\left[\left(\frac{A}{2}+\omega_n\right)^2+\left|\frac{B}{2}\right|^2\right]^{1/2}, \\ c_1&=\frac{1}{\sqrt{2}}\left[1\pm\frac{(A/2)-\omega_n}{\omega_\alpha}\right]^{1/2}, \\ c_2&=-\frac{1}{\sqrt{2}}\left[1\mp\frac{(A/2)-\omega_n}{\omega_\alpha}\right]^{1/2}, \\ c_3&=\frac{1}{\sqrt{2}}\left[1+\frac{(A/2)+\omega_n}{\omega_\beta}\right]^{1/2}, \\ c_4&=-\frac{1}{\sqrt{2}}\left[1-\frac{(A/2)+\omega_n}{\omega_\beta}\right]^{1/2}. \end{aligned} \tag{A4}$$

The upper and lower signs in the definition of c_1 and c_2 correspond to the case of $A/2>|\omega_n|$ and $A/2<\omega_n$, respectively. Clearly ω_α, ω_β, and the c_i's depend on the molecular orientation, i.e., the $\mathscr{H}_0$ basis is orientation dependent, whereas the $|S_zI_z\rangle$ basis is not.

a. Effect of the pulse

Assuming a short and intense pulse, we can ignore the effects of the spin Hamiltonian $\hat{H}$ and of the relaxation during the pulse. During the pulse, the density matrix evolves according to

$$\frac{d\rho}{dt}=-i[\hat{e}(t),\rho], \tag{A6}$$

where $\hat{e}(t)$ is the irradiating microwave pulse with intensity $B_1=\omega_1/\gamma_e$ and phase ϕ. We have

$$\hat{e}(t)=\gamma_eB_1(S_x\cos\phi+S_y\sin\phi)=\frac{\omega_1}{2}(e^{-i\phi}S_++e^{i\phi}S_-). \tag{A7}$$

The formal solution can be written for a pulse of duration t_p as

$$\rho(t_0+t_p)=\exp(-i\hat{e}t_p)\rho(t_0)\exp(i\hat{e}t_p), \tag{A8}$$

where the exponential operator may be written as

$$\exp(i\hat{e}t_p)=\begin{bmatrix} \cos(\theta/2)\mathbf{1} & i\sin(\theta/2)e^{-i\phi}\mathbf{1} \\ i\sin(\theta/2)e^{i\phi}\mathbf{1} & \cos(\theta/2)\mathbf{1} \end{bmatrix} \quad \text{in the } |S_zI_z\rangle \text{ basis.} \tag{A9}$$

Here $\mathbf{1}$ is the 2×2 unit matrix and $\theta=\omega_1t_p$.

Converting this matrix representation of the exponential operator into the $\mathscr{H}_0$ basis, we have

$$\exp(i\hat{e}t_p)=\begin{pmatrix}\cos(\theta/2)\mathbf{1} & i\sin(\theta/2)e^{-i\phi}\mathbf{M}\\ i\sin(\theta/2)e^{i\phi}\mathbf{M}^{\dagger} & \cos(\theta/2)\mathbf{1}\end{pmatrix}\quad\text{in the } \mathscr{H}_0 \text{ basis,} \tag{A10}$$

where

$$\mathbf{M}=\mathbf{T}_{\alpha}^{\dagger}\mathbf{T}_{\beta}=\begin{pmatrix}m_1 & m_2\\ -m_2 & m_1\end{pmatrix}\equiv\begin{pmatrix}c_1c_3+c_2c_4 & c_1c_4-c_2c_3\\ c_2c_3-c_1c_4 & c_1c_3+c_2c_4\end{pmatrix}. \tag{A11}$$

Since the pulse propagator depends simply on the m_i's, the final signal observed for any arbitrary pulse sequence can be expressed in terms of the m_i's. It is therefore convenient to express the m_i's and the associated k's by some useful relations in terms of parameters in the spin Hamiltonian. They are given in Table III. Note that the case of $A/2>\omega_n$ in Table III can be obtained from the case of $A/2<\omega_n$ just by interchanging ω_+, ω_- and changing the sign of ω_α.

TABLE III. Relevant coefficients for nuclear modulation.

Constants	$\lvert A/2\rvert \gtrless \lvert\omega_n\rvert$
$k=4m_1^2m_2^2=\left(\frac{\omega_n\lvert B\rvert}{\omega_\alpha\omega_\beta}\right)^2$	The same
$k_+=m_1^4=\frac{1}{2}\left(1-\frac{k}{2}+\sqrt{1-k}\right)$	$\left(\frac{\omega_n^2-\omega_\pm^2}{\omega_\alpha\omega_\beta}\right)^2$
$k_-=m_2^4=\frac{1}{2}\left(1-\frac{k}{2}-\sqrt{1-k}\right)$	$\left(\frac{\omega_n^2-\omega_\mp^2}{\omega_\alpha\omega_\beta}\right)^2$
m_1^2	$\frac{1}{2}\left(1\mp\frac{\omega_n^2-(A/2)^2-\lvert B/2\rvert^2}{\omega_\alpha\omega_\beta}\right)$
m_2^2	$\frac{1}{2}\left(1\pm\frac{\omega_n^2-(A/2)^2-\lvert B/2\rvert^2}{\omega_\alpha\omega_\beta}\right)$

where $\omega_\pm=\frac{1}{2}(\omega_\alpha\pm\omega_\beta)$

2. The density matrix in the basis that diagonalizes the Hamiltonian in Liouville space (Ref. 46)

The evolution of the density matrix ρ is governed by the Stochastic–Liouville equation (SLE)[33]

$$\frac{d}{dt}\rho(\Omega,t)=-i[\hat{H},\rho(\Omega,t)]-\tilde{\Gamma}[\rho(\Omega,t)-\rho_0(\Omega)], \tag{A12}$$

$\hat{H}$ is the spin Hamiltonian operator, and $\tilde{\Gamma}$ is a relaxation superoperator. Throughout the paper, "$\hat{\ }$" and "$\tilde{\ }$" will be used to denote the operator and the superoperator, respectively. The bold character will represent the matrix for the relevant operator. The difference between the time-dependent density matrix and the equilibrium density matrix ρ_0 is denoted as $\chi(t)\equiv\rho(t)-\rho_0$, and enables us to rewrite Eq. (A12) as

$$\frac{d}{dt}\chi=-i\tilde{H}\chi(t)-\tilde{\Gamma}\chi(t), \tag{A13}$$

since $\rho_0=[\exp(-\hbar\hat{H}/kT)]/\{\mathrm{Tr}[\exp(-\hbar\hat{H}/kT)]\}$ and thus commutes with $\hat{H}$. This can be rewritten in matrix notation in Liouville space as follows:

$$\frac{d}{dt}\mathbf{X}=-i\tilde{\mathbf{H}}\mathbf{X}-\tilde{\Gamma}\mathbf{X}, \tag{A14}$$

where $\mathbf{X}$ is a vector of dimension 16 whose elements are just the 16 density matrix elements.

The Hamiltonian commutator superoperator $\tilde{\mathbf{H}}$ in Liouville space corresponding to the $|S_zI_z\rangle$ basis can be shown to be block diagonal in four blocks

$$\tilde{\mathbf{H}}=\mathrm{Diag}\{\tilde{H}_1,\tilde{H}_2,\tilde{H}_3,\tilde{H}_4\},$$

$$\tilde{H}_1=\begin{pmatrix}\chi_{12} & \chi_{21} & \chi_{11} & \chi_{22}\\ H_{11}-H_{22} & 0 & -H_{12} & H_{12}\\ 0 & H_{22}-H_{11} & H_{21} & -H_{21}\\ -H_{21} & H_{12} & 0 & 0\\ H_{21} & -H_{12} & 0 & 0\end{pmatrix},\quad \tilde{H}_2=\begin{pmatrix}\chi_{33} & \chi_{44} & \chi_{34} & \chi_{43}\\ 0 & 0 & -H_{43} & H_{34}\\ 0 & 0 & H_{43} & -H_{34}\\ -H_{34} & H_{34} & H_{33}-H_{44} & 0\\ H_{43} & -H_{43} & 0 & H_{44}-H_{33}\end{pmatrix}, \tag{A15}$$

$$\tilde{H}_3=\begin{pmatrix}\chi_{13} & \chi_{14} & \chi_{23} & \chi_{24}\\ H_{11}-H_{33} & -H_{43} & H_{12} & 0\\ -H_{34} & H_{11}-H_{44} & 0 & H_{12}\\ H_{12} & 0 & H_{22}-H_{33} & -H_{43}\\ 0 & H_{21} & -H_{34} & H_{22}-H_{44}\end{pmatrix},\quad \tilde{H}_4=\begin{pmatrix}\chi_{31} & \chi_{41} & \chi_{32} & \chi_{42}\\ H_{33}-H_{11} & H_{34} & -H_{21} & 0\\ H_{43} & H_{44}-H_{11} & 0 & -H_{21}\\ -H_{12} & 0 & H_{33}-H_{22} & H_{34}\\ 0 & -H_{12} & H_{43} & H_{44}-H_{22}\end{pmatrix},$$

where the matrix elements H_{ij} are given in Eq. (A2). $\tilde{H}_1$ and $\tilde{H}_2$ are in the space spanned by the diagonal and pseudodiagonal elements of χ for $M_s=+1/2$ and $-1/2$, respectively. $\tilde{H}_3$ and $\tilde{H}_4$ are in the space spanned by the off-diagonal elements of χ corresponding to the allowed and forbidden ESR transitions. Note that $\tilde{H}_4=-\tilde{H}_3^{\mathrm{tr}}$. This Hamiltonian superoperator $\tilde{\mathbf{H}}$ is diagonalized by the unitary matrix $\mathbf{U}$,[47]

$$\mathbf{U}^{\dagger}\tilde{\mathbf{H}}\mathbf{U}=\tilde{\mathbf{F}}, \quad \mathbf{U}_{\mu\nu,mn}=\mathbf{T}_{\mu m}\mathbf{T}^{\dagger}_{n\nu}. \tag{A16}$$

$\tilde{\mathbf{F}}$ is the matrix representation of $\tilde{H}$ in the $\mathscr{H}_0$ basis. Therefore it is diagonal and each nonzero element is a transition frequency. The unitary transforms $\mathbf{U}$ and $\mathbf{T}$ are related by Eq. (A16). The matrix elements for $\tilde{\mathbf{F}}$ and $\mathbf{U}$ are given in Eqs. (A17) and (A18)

$$\begin{aligned}\tilde{\mathbf{F}}=\mathrm{Diag}\{&\omega_{\alpha},-\omega_{\alpha},0,0,0,0,-\omega_{\beta},\omega_{\beta};\\ &C+\omega_{+},C+\omega_{-},C-\omega_{-},C-\omega_{+};\\ &-C-\omega_{+},-C-\omega_{-},-C+\omega_{-},-C+\omega_{+}\}\end{aligned} \tag{A17}$$

in the $\mathscr{H}_0$ basis consisting of

$$\{\chi_{ab},\chi_{ba},\chi_{aa},\chi_{bb},\chi_{cc},\chi_{dd},\chi_{cd},\chi_{dc},\chi_{ac},\chi_{ad},\chi_{bc},\chi_{bd},\chi_{ca},\chi_{da},\chi_{cb},\chi_{db}\},$$

$$\mathbf{U}=\mathrm{Diag}\{\mathbf{U}_1,\mathbf{U}_2,\mathbf{U}_3,\mathbf{U}_3\}, \quad \mathbf{U}_1=\begin{array}{c}\begin{matrix}\chi_{12} & \chi_{21} & \chi_{11} & \chi_{22}\end{matrix}\\ \begin{pmatrix} c_1^2 & -c_2^2 & -c_1c_2 & c_1c_2\\ -c_2^2 & c_1^2 & -c_1c_2 & c_1c_2\\ c_1c_2 & c_1c_2 & c_1^2 & c_2^2\\ -c_1c_2 & -c_1c_2 & c_2^2 & c_1^2\end{pmatrix}\end{array}\begin{matrix}\chi_{ab}\\ \chi_{ba}\\ \chi_{aa}\\ \chi_{bb}\end{matrix},$$

$$\mathbf{U}_2=\begin{array}{c}\begin{matrix}\chi_{33} & \chi_{44} & \chi_{34} & \chi_{43}\end{matrix}\\ \begin{pmatrix} c_3^2 & c_4^2 & c_3c_4 & c_3c_4\\ c_4^2 & c_3^2 & -c_3c_4 & -c_3c_4\\ -c_3c_4 & c_3c_4 & c_3^2 & -c_4^2\\ -c_3c_4 & c_3c_4 & -c_4^2 & c_3^2\end{pmatrix}\end{array}\begin{matrix}\chi_{cc}\\ \chi_{dd}\\ \chi_{cd}\\ \chi_{dc}\end{matrix}, \quad \mathbf{U}_3=\begin{array}{c}\begin{matrix}\chi_{13} & \chi_{14} & \chi_{23} & \chi_{24}\end{matrix}\\ \begin{pmatrix} c_1c_3 & c_1c_4 & c_2c_3 & c_2c_4\\ -c_1c_4 & c_1c_3 & -c_2c_4 & c_2c_3\\ -c_2c_3 & -c_2c_4 & c_1c_3 & c_1c_4\\ c_2c_4 & -c_2c_3 & -c_1c_4 & c_1c_3\end{pmatrix}\end{array}\begin{matrix}\chi_{ac}\\ \chi_{ad}\\ \chi_{bc}\\ \chi_{bd}\end{matrix}. \tag{A18}$$

In Eq. (A18), we indicate the basis of U in terms of the $|S_zI_z\rangle$ and the $\mathscr{H}_0$ basis vectors.

3. Spin relaxation

The relaxation superoperator $\tilde{\Gamma}$ will, in general, display orientation dependence. In problems which involve orientational motions, $\tilde{\Gamma}$ becomes a rotational diffusion operator and it does not commute with the orientation-dependent terms in $\hat{H}$. For the present experiments on malonic acid crystals, we assume that phonon modulation of hf and g tensors leads to spin relaxation that can be described by the Redfield equation applicable for motional narrowing [i.e., these are the fast phonon modes; slow modes would have different effects (cf. Sec. IV D)]. Then Eq. (A1) for $\hat{H}$ is the thermal average over these fluctuations, and the Redfield relaxation matrix $\mathbf{R}$ is composed from the small fluctuations in these terms, which are summarized in Table IV. Note that in this approach, the density matrix for each orientation of the molecular magnetic tensors relative to the lab frame specified by $\Omega=(0,\beta,\gamma)$ [cf. Eq. (2)] is taken as uncoupled from all others (this simplification would not be strictly correct if for example there were torsional oscillations). Then the Redfield relaxation matrix $\mathbf{R}$ will depend on the orientation of the single crystal. Thus we write a separate $\mathbf{R}$ for each value of Ω in the corresponding $\mathscr{H}_0$ basis. (This is a local approach as opposed to the global approach utilized in motional narrowing problems in which $\mathbf{R}$ is written in the $|S_zI_z\rangle$ basis.) Thus we formulate the effects of spin relaxation phenomenologically by the Redfield equation for arbitrary orientation Ω,[48]

$$\frac{d\chi_{\alpha\alpha'}}{dt}=-i\omega_{\alpha\alpha'}\chi_{\alpha\alpha'}+\sum_{\beta,\beta'}R_{\alpha\alpha',\beta\beta'}\chi_{\beta\beta}, \tag{A19}$$

where $\alpha,\alpha',\beta,\beta'$ are the spin quantum numbers that represent the eigenstates of the Hamiltonian $\hat{H}$ expressed by Eq. (A1). At this stage, one has the choice of calculating the full relaxation matrix in the $|S_zI_z\rangle$ basis (which is relatively easy) and then transform to the $\mathscr{H}_0$ basis using the transformation defined by Eq. (A18), or alternatively to evaluate the relaxation matrix directly in the $\mathscr{H}_0$ basis, which is somewhat more difficult. The latter choice of basis does have the virtue that the only important contributions come from the terms that satisfy $\omega_{\alpha\alpha'}\approx\omega_{\beta\beta'}$. This simplification does not apply in the $|S_zI_z\rangle$ basis prior to its transformation. Note that all terms in Eq. (A19) are functions of Ω, although we do not display this dependence for simplicity in presentation. In this Liouville space spanned by the $\mathscr{H}_0$ basis set, the diagonal and the off-diagonal parts of the relaxation matrix are

$$\begin{aligned}&\tilde{R}_{\alpha\beta,\alpha\beta}=-(1/T_2)_{\alpha\beta}, \quad \text{off diagonal},\\ &\tilde{R}_{\alpha\alpha,\beta\beta}=W_{\beta\alpha}, \quad \tilde{R}_{\beta\beta,\alpha\alpha}=W_{\alpha\beta}, \quad \text{diagonal},\\ &\tilde{R}_{\alpha\alpha,\alpha\alpha}=-\sum_{\gamma\neq\alpha}W_{\alpha\gamma}, \quad \text{diagonal}.\end{aligned} \tag{A20}$$

In the above discussion, we have emphasized the role of modulation of the dominant interactions in the spin Hamiltonian. In an actual malonic acid crystal, there are also matrix protons which interact weakly by dipolar interactions with the unpaired electrons of the malonic acid

TABLE IV. Illustration of the effect of fluctuation of the various terms in the spin Hamiltonian on the relaxation rates.

	$\mathcal{F}^{a,b}$	$\mathcal{A}^{c,d}$	$\lvert\mathcal{A}_{ac}\rvert^2$	$\lvert\mathcal{A}_{bd}\rvert^2$	$\lvert\mathcal{A}_{ad}\rvert^2$	$\lvert\mathcal{A}_{bc}\rvert^2$	$\lvert\mathcal{A}_{ab}\rvert^{2,e}$	$\lvert\mathcal{A}_{aa}\rvert^2$, $\lvert\mathcal{A}_{bb}\rvert^{2,e}$
Isotropic g	$\frac{\beta_e B_0}{\hbar}\delta g$	S_z						$\frac{1}{4}$
Anisotropic g	$\delta F\frac{1}{2}(3\cos^2\beta-1)+\delta F^{(2)}\sin^2\beta\cos(2\gamma)$	S_z						$\frac{1}{4}$
	$\delta F\frac{3}{8}\sin(2\beta)-\delta F^{(2)}\frac{1}{4}\sin(2\beta)\cos(2\gamma)$	$S_+ + S_-$	m_1^2	m_1^2	m_2^2	m_2^2		
Isotropic hf	$-\frac{\gamma_e}{\hbar}\delta a$	S_zI_z					$\frac{1}{4}\{\mathrm{Re}(c_1^*c_2)\}^2$	$\frac{1}{16}(\lvert c_1\rvert^2-\lvert c_2\rvert^2)$
		$\frac{1}{2}(S_+I_- + S_-I_+)$	$\frac{1}{4}\lvert c_2^*c_3\rvert^2$	$\frac{1}{4}\lvert c_1^*c_4\rvert^2$	$\frac{1}{4}\lvert c_2^*c_4\rvert^2$	$\frac{1}{4}\lvert c_1^*c_3\rvert^2$		
Anisotropic hf	$-\frac{\gamma_e}{\hbar}\left[\delta D\frac{1}{2}(3\cos^2\beta-1)+\delta D^{(2)}\sin^2\beta\cos(2\gamma)\right]$	S_zI_z					$\frac{1}{4}\{\mathrm{Re}(c_1^*c_2)\}^2$	$\frac{1}{16}(\lvert c_1\rvert^2-\lvert c_2\rvert^2)$
		$-\frac{1}{4}(S_+I_- + S_-I_+)$	$\frac{1}{16}\lvert c_2^*c_3\rvert^2$	$\frac{1}{16}\lvert c_1^*c_4\rvert^2$	$\frac{1}{16}\lvert c_2^*c_4\rvert^2$	$\frac{1}{16}\lvert c_1^*c_3\rvert^2$		
	$-\frac{\gamma_e}{\hbar}\left[\delta D\frac{3}{8}\sin(2\beta)-\delta D^{(2)}\frac{1}{4}\sin(2\beta)\cos(2\gamma)\right]$	$S_zI_+ + S_zI_-$					$\frac{1}{4}(\lvert c_1\rvert^2-\lvert c_2\rvert^2)^2$	$\{\mathrm{Re}(c_1^*c_2)\}^2$
		$S_+I_z + S_-I_z$	$\frac{1}{4}\lvert c_1^*c_3-c_2^*c_4\rvert^2$	$\frac{1}{4}\lvert c_1^*c_3-c_2^*c_4\rvert^2$	$\frac{1}{4}\lvert c_1^*c_4+c_2^*c_3\rvert^2$	$\frac{1}{4}\lvert c_1^*c_4+c_2^*c_3\rvert^2$		
	$-\frac{\gamma_e}{\hbar}\left[\delta D\frac{3}{8}\sin^2\beta-\delta D^{(2)}\frac{1}{4}(1+\cos^2\beta)\cos(2\gamma)\right]$	$S_+I_+ + S_-I_-$	$\lvert c_1^*c_4\rvert^2$	$\lvert c_2^*c_3\rvert^2$	$\lvert c_1^*c_3\rvert^2$	$\lvert c_2^*c_4\rvert^2$		

[a]The interaction constants ($\delta g,\delta a,\delta F,\delta F^{(2)},\delta D,\delta D^{(2)}$) are the time-dependent deviations from the average values [e.g., $\delta g=g(t)-\bar{g}$].

[b]For the orientations chosen in the experiment ($\gamma=0°$ or $90°$), $\sin(2\gamma)=0$ and $\cos(2\gamma)=\pm1$. For an arbitrary angle, those terms with $F^{(2)}$ or $D^{(2)}$ and $S_\pm$ or $I_\pm$ become a complex number whose imaginary part is proportional to $\sin(2\gamma)$. This general case is not shown in the table for brevity.

[c]The quantities m_1 and m_2 are given in Table III; c_i are given by Eq. (A5).

[d]For compactness, we have not explicitly included cross terms between the various types of terms. These can be written down simply in terms of the products $\mathcal{F}^q\mathcal{F}^r$, $r\neq q$ in Eqs. (B3) and (B4). $\mathcal{A}^q_{\alpha\gamma}\mathcal{A}^r_{\alpha\gamma}$ may also readily be written down; e.g., the cross term from S_+ due to the anisotropic g tensor with $-\frac{1}{4}S_+I_-$ from the anisotropic hf term is $2m_1\mathrm{Re}(\frac{1}{4}c_2^*c_3)$ for $\mathcal{A}^g_{ac}\mathcal{A}^{hf}_{ca}+\mathcal{A}^{hf}_{ac}\mathcal{A}^g_{ca}$.

[e]$\mathcal{A}_{cd}$, $\mathcal{A}_{cc}$, and $\mathcal{A}_{dd}$ are obtained by substituting $c_1\rightarrow c_3$ and $c_2\rightarrow c_4$ in the entries below.

radical (cf. Sec. IV D). These can contribute to T_{2e} and T_{2n} by spin diffusion, especially at low temperatures.[38,39]

If the electron-spin concentration is not very dilute, then electron–electron dipolar (EED) interactions can play a role, as also mentioned in Sec. IV D. Here we emphasize the mutual electron-spin flip flops due to the $S_{1\pm}S_{2\mp}$ terms which can transfer spins between the two proton hf lines of malonic acid.[11,39] The formal properties of this spin interaction are the same as Heisenberg exchange (HE),[11] so we take advantage of this below and nominally consider the HE mechanism, although a rigorous theory would model the magnitudes of the terms based on EED terms. The $S_{1\pm}S_{2\mp}$ terms, in causing spin transfer between the hf lines, do not conserve energies of the order of A [cf. Eq. (A1)], so they must be assisted by phonon modulation of this interaction. (Note that phonon modulation of $S_{1\pm}S_{2z}$ and $S_{1\pm}S_{2\pm}$ type terms would contribute to T_{1e} as well as W_x for certain orientations.) The theory for relaxation from HE[11,36] is most readily applied in the $|S_zI_z\rangle$ basis, followed by transformation by $\mathbf{U}$ into the $\mathscr{H}_0$ basis.

In order to simplify the analysis, we shall choose to introduce the following equalities, which, however, are not general as can be seen from Appendix B and illustrated in Table IV. Nevertheless, they capture the essence of the relaxation problem, while permitting tractable analytic solutions to the problem

(i) $T_{2e}=(T_2)_{ac}=(T_2)_{bd}=(T_2)_{ad}=(T_2)_{bc}$,

$T_{2n}=(T_2)_{ab}=(T_2)_{cd}$,

(ii) $W_e=W_{ac}=W_{bd}$,

$W_n=W_{ab}=W_{cd}$,

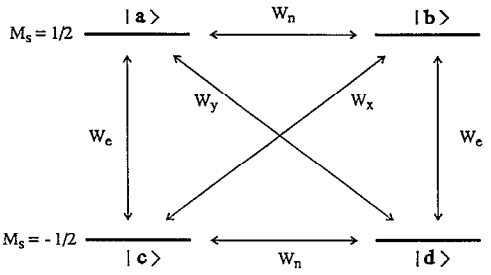

FIG. 16. The relaxation pathways defined in the $\mathscr{H}_0$ basis

$$W_x=W_{bc}=W_{ad}. \tag{A21}$$

[Considering only g and hf tensor terms, (i) of Eq. (A21) would be true if g-tensor contributions dominate T_{2e} and T_{2n}; (ii) of Eq. (A21) also requires the tilt angle $\beta\cong 0$, so that $B\cong 0$. We can similarly neglect the complication in the treatment of HE requiring its transformation by $\mathbf{U}$, by either assuming $B\cong 0$ or else $|\omega_n|\ll|A/2|$ so $c_3\cong c_1$, and $c_4\cong c_2$. The expressions written below for HE are simplified in this manner.] The relaxation scheme is illustrated in Fig. 16. The relaxation matrix $\tilde{\mathbf{R}}$ in the $\mathscr{H}_0$ basis becomes:

$$\tilde{\mathbf{R}}=\mathrm{Diag}\left\{-\frac{1}{T_{2n}},-\frac{1}{T_{2n}},\mathbf{W},-\frac{1}{T_{2n}},-\frac{1}{T_{2n}},-\frac{1}{T_{2e}},\ldots,-\frac{1}{T_{2e}}\right\} \tag{A22}$$

in the same basis as $\tilde{\mathbf{F}}$ [Eq. (A17)]. Note the eigenvalue $-1/T_{2e}$ is repeated eight times in Eq. (A22). $\mathbf{W}$ is the 4×4 matrix corresponding to the diagonal part of χ,

$$\mathbf{W}=\begin{pmatrix} \chi_{aa} & \chi_{bb} & \chi_{cc} & \chi_{dd} \\ -W_e-W_n-W_x-\omega_{\mathrm{HE}}/4 & W_n+\omega_{\mathrm{HE}}/4 & W_e+\omega_{\mathrm{HE}}/4 & W_x-\omega_{\mathrm{HE}}/4 \\ W_n+\omega_{\mathrm{HE}}/4 & -W_e-W_n-W_x-\omega_{\mathrm{HE}}/4 & W_x-\omega_{\mathrm{HE}}/4 & W_e+\omega_{\mathrm{HE}}/4 \\ W_e+\omega_{\mathrm{HE}}/4 & W_x-\omega_{\mathrm{HE}}/4 & -W_e-W_n-W_x-\omega_{\mathrm{HE}}/4 & W_n+\omega_{\mathrm{HE}}/4 \\ W_x-\omega_{\mathrm{HE}}/4 & W_e+\omega_{\mathrm{HE}}/4 & W_n+\omega_{\mathrm{HE}}/4 & -W_e-W_n-W_x-\omega_{\mathrm{HE}}/4 \end{pmatrix}. \tag{A23}$$

Thus, in the $\mathscr{H}_0$ basis, we may write Eq. (A19) in matrix form as [cf. Eq. (A14)]

$$\frac{d\mathbf{X}}{dt}=(-i\tilde{\mathbf{F}}+\tilde{\mathbf{R}})\mathbf{X}. \tag{A24}$$

The final solutions may thus be obtained by diagonalizing $(-i\tilde{\mathbf{F}}+\tilde{\mathbf{R}})$. However, by virtue of Eqs. (A17), (A22), and (A23), only the 4×4 subspace of diagonal elements χ_{ii} is still nondiagonal. Since $\tilde{\mathbf{F}}$ in this subspace is just the null matrix, it is just necessary to diagonalize $\mathbf{W}$ given by Eq. (A23) to obtain the normal modes of relaxation. That is,

$$\mathbf{S}_w^{\dagger}\mathbf{W}\mathbf{S}_w=\Lambda_w=\{0,\lambda_4,\lambda_5,\lambda_6\}, \tag{A25}$$

where λ_4, λ_5, and λ_6 are negative real and $\lambda_3=0$, corresponding to the conservation of total probability. In this normal mode basis, $(-i\tilde{\mathbf{F}}+\tilde{\mathbf{R}})$ is a diagonal matrix and can be written as

$$\Lambda=\mathrm{Diag}\left\{-i\omega_\alpha-\frac{1}{T_{2n}},i\omega_\alpha-\frac{1}{T_{2n}},0,\lambda_4,\lambda_5,\lambda_6,i\omega_\beta-\frac{1}{T_{2n}},\right.$$

$$\left.-i\omega_\beta-\frac{1}{T_{2n}},-i(C+\omega_+)-\frac{1}{T_{2e}},-i(C+\omega_-)-\frac{1}{T_{2e}},\right.$$

$$-i(C-\omega_-)-\frac{1}{T_{2e}},-i(C-\omega_+)-\frac{1}{T_{2e}},$$

$$i(C+\omega_+)-\frac{1}{T_{2e}},i(C+\omega_-)-\frac{1}{T_{2e}},i(C-\omega_-)$$

$$-\frac{1}{T_{2e}},i(C-\omega_+)-\frac{1}{T_{2e}}\Big\}. \tag{A26}$$

Note that for the complex eigenvalues corresponding to the various transitions, the real parts are the homogeneous linewidths and the imaginary parts are the transition frequencies. The values of λ_4, λ_5, λ_6 and of $\mathbf{S}_w$ are quite complicated, in general. However with the assumptions in Eq. (A21), we can get a very simple analytical expression

$$\mathbf{S}_w=\frac{1}{2}\begin{pmatrix}1&1&1&1\\1&-1&1&-1\\1&1&-1&-1\\1&-1&-1&1\end{pmatrix}, \tag{A27}$$

$$\{\lambda_4,\lambda_5,\lambda_6\}=\{-2W_n-2W_x,-2W_e-2W_x,$$
$$-2W_e-2W_n-\omega_{\mathrm{HE}}\}.$$

In summary, $(-i\tilde{\mathbf{H}}+\tilde{\mathbf{R}})$ expressed most conveniently in the $|S_zI_z\rangle$ basis is transformed into the normal mode basis by two consecutive unitary transformations $\mathbf{U}$ followed by $\mathbf{S}$,

$$(\mathbf{US})^\dagger(-i\tilde{\mathbf{H}}+\tilde{\mathbf{R}})(\mathbf{US})=\mathbf{\Lambda}. \tag{A28}$$

The evolution of the density matrix in the absence of the radiation field then obeys the simple "complex-exponential" form

$$\bar{\mathbf{X}}(t_0+t)=\exp(-\mathbf{\Lambda}t)\bar{\mathbf{X}}(t_0), \tag{A29}$$

where $\bar{\mathbf{X}}=(\mathbf{US})^\dagger\mathbf{X}$.

4. The pulse propagator in Liouville space

Equation (A8) can be rewritten in Liouville space as follows:

$$\rho_{\alpha\alpha'}(t_0+t_p)=\sum_{\beta,\beta'}\tilde{\mathbf{P}}_{\alpha\alpha',\beta\beta'}\rho_{\beta\beta'} \tag{A30}$$

with the pulse propagator superoperator $\tilde{\mathbf{P}}$,

$$\tilde{\mathbf{P}}_{\alpha\alpha',\beta\beta'}=[\exp(-i\hat{\epsilon}t_p)]_{\alpha\beta}[\exp(i\hat{\epsilon}t_p)]_{\beta'\alpha'}. \tag{A31}$$

We can rewrite Eq. (A30) in matrix form

$$\mathbf{X}(t_0+t_p)=\tilde{\mathbf{P}}\mathbf{X}(t_0)+(\tilde{\mathbf{P}}-\mathbf{1})\rho_0. \tag{A32}$$

$\tilde{\mathbf{P}}$ given by Eqs. (A9) and (A31) can be expressed most conveniently in the $|S_zI_z\rangle$ basis in the order shown in Eq. (A15)

$$\tilde{\mathbf{P}}=\begin{pmatrix}\cos^2(\theta/2)\mathbf{1}&P_{12}&iP_{13}&iP_{14}\\P_{12}^\dagger&\cos^2(\theta/2)\mathbf{1}&iP_{23}&iP_{24}\\iP_{13}^\dagger&iP_{23}^\dagger&\cos^2(\theta/2)\mathbf{1}&P_{34}\\iP_{14}^\dagger&iP_{24}^\dagger&P_{34}^\dagger&\cos^2(\theta/2)\mathbf{1}\end{pmatrix},$$

$$P_{12}=\sin^2\left(\frac{\theta}{2}\right)\begin{pmatrix}0&0&1&0\\0&0&0&1\\1&0&0&0\\0&1&0&0\end{pmatrix},\quad P_{13}=\frac{1}{2}\sin\theta e^{i\phi}\begin{pmatrix}0&1&0&0\\0&0&1&0\\1&0&0&0\\0&0&0&1\end{pmatrix},$$

$$P_{14}=-\frac{1}{2}\sin\theta e^{-i\phi}\begin{pmatrix}0&0&1&0\\0&1&0&0\\1&0&0&0\\0&0&0&1\end{pmatrix},\quad P_{23}=-\frac{1}{2}\sin\theta e^{i\phi}\begin{pmatrix}1&0&0&0\\0&0&0&1\\0&1&0&0\\0&0&1&0\end{pmatrix}, \tag{A33}$$

$$P_{24}=\frac{1}{2}\sin\theta e^{-i\phi}\begin{pmatrix}1&0&0&0\\0&0&0&1\\0&0&1&0\\0&1&0&0\end{pmatrix},\quad P_{34}=\sin^2\left(\frac{\theta}{2}\right)e^{-2i\phi}\begin{pmatrix}1&0&0&0\\0&0&1&0\\0&1&0&0\\0&0&0&1\end{pmatrix}.$$

Transforming into the $\mathscr{H}_0$ and normal mode basis, we get

$$\bar{\mathbf{X}}(t_0+t_p)=\bar{\mathbf{P}}\bar{\mathbf{X}}(t_0)+(\bar{\mathbf{P}}-\mathbf{1})\bar{\rho}_0 \tag{A34}$$

with $\bar{\mathbf{P}}=(\mathbf{US})^{\dagger}\tilde{\mathbf{P}}(\mathbf{US})$ and $\bar{\rho}_0=(\mathbf{US})^{\dagger}\rho_0$. Using Eqs. (A29) and (A34), the evolution of the density matrix can be calculated for any pulse sequence. Equations (5) and (7) in the main text for SECSY ESR and 2D ELDOR plus stimulated SECSY, respectively, were derived by this procedure.

APPENDIX B: ORIENTATION-DEPENDENT SPIN RELAXATION

The fluctuating time-dependent perturbation leading to the relaxation can be written in general form as follows[49]:

$$\mathscr{H}_1(t)=\sum_q \mathscr{F}_i^q \mathscr{A}_i^q, \tag{B1}$$

where $\mathscr{A}_i$ are the spin operators in the lab frame and $\mathscr{F}_i$ are the time-dependent fluctuating parts of the Hamiltonian, which are defined in the molecular frame and transformed into the lab frame.

For the $\mathscr{H}_0$ basis, with a significant hf tensor, there are no degenerate energy levels and transitions, so we have only the diagonal elements for the T_2-type relaxation, i.e.,

$$\begin{aligned}(T_2^{-1})_{\alpha\beta}&=-R_{\alpha\beta,\alpha\beta}\\&=\int_0^{\infty} d\tau\overline{\omega_{\alpha\beta}(t)\omega_{\alpha\beta}(t+\tau)}\\&\quad+\frac{1}{2}\left(\sum_{\gamma\neq\alpha}W_{\alpha\gamma}+\sum_{\gamma\neq\beta}W_{\beta\gamma}\right),\end{aligned} \tag{B2}$$

where $\omega_{\alpha\beta}(t)=[\mathscr{H}_1(t)_{\alpha\alpha}-\mathscr{H}_1(t)_{\beta\beta}]$, and the first term on the right-hand side of Eq. (B2) is usually taken as $T_2'^{-1})_{\alpha\beta}$.

So

$$\begin{aligned}&\int_0^{\infty} d\tau\overline{\omega_{\alpha\beta}(t)\omega_{\alpha\beta}(t+\tau)}\\&=\sum_{q,r}(\mathscr{A}_{\alpha\alpha}^q-\mathscr{A}_{\beta\beta}^q)(\mathscr{A}_{\alpha\alpha}^r-\mathscr{A}_{\beta\beta}^r)\\&\quad\times\int_{-\infty}^{\infty} d\tau\overline{\mathscr{F}^q(t)\mathscr{F}^{r*}(t+\tau)}\end{aligned} \tag{B3}$$

and the transition probabilities $W_{\alpha\gamma}$ which provide T_1-type relaxation and also contribute to T_2 can be written as

$$\begin{aligned}W_{\alpha\gamma}=R_{\alpha\alpha,\gamma\gamma}&=\sum_{q,r}\mathscr{A}_{\alpha\gamma}^q\mathscr{A}_{\gamma\alpha}^r\int_{-\infty}^{\infty}\overline{\mathscr{F}^q(t)\mathscr{F}^{r*}(t+\tau)}\\&\quad\times\exp(-i\omega_{\alpha\gamma}\tau)d\tau.\end{aligned} \tag{B4}$$

The specific role of the g and hf tensors is illustrated in Table IV for the $\mathscr{H}_0$ basis. Note that not only are the $\mathscr{F}^q$ orientation dependent, but the $\mathscr{A}_{\alpha\gamma}^q$ can also show substantial orientation dependence. Utilizing Table IV and Eqs. (B2)–(B4), it is readily possible to write down all the relevant (orientation-dependent) T_2's and $W_{\alpha\gamma}$'s. Whereas this leads in general to complex expressions not amenable to analytical solution, our general computer program permits the calculation of the 2D-ESR spectrum for any case of relaxation in the high temperature limit.

[1] W. B. Mims, K. Nassau, and J. D. McGee, Phys. Rev. **123**, 2059 (1961).
[2] J. A. Cowen and D. E. Kaplan, Phys. Rev. **124**, 1098 (1961).
[3] L. G. Rowan, E. L. Hahn, and W. B. Mims, Phys. Rev. A **137**, 61 (1965).
[4] W. B. Mims, Phys. Rev. B **5**, 2409 (1972).
[5] L. Kevan, in *Time Domain Electron Spin Resonance*, edited by L. Kevan and R. N. Schwartz (Wiley, New York, 1979).
[6] A. Schweiger, in *Modern Pulsed and Continuous Wave Electron Spin Resonance*, edited by L. Kevan and M. K. Bowman (Wiley, New York, 1990).
[7] L. Kevan, in *Modern Pulsed and Continuous Wave Electron Spin Resonance*, edited by L. Kevan and M. K. Bowman (Wiley, New York, 1990).
[8] W. B. Mims and J. Peisach, in *Advanced EPR*, edited by A. J. Hoff (Elsevier, Amsterdam, 1989).
[9] S. A. Dikanov and A. V. Astashkin, in *Advanced EPR*, edited by A. J. Hoff (Elsevier, Amsterdam, 1989).
[10] D. J. Singel, in *Advanced EPR*, edited by A. J. Hoff (Elsevier, Amsterdam, 1989).
[11] J. H. Freed, in *Multiple Electron Resonance Spectroscopy*, edited by M. Dorio and J. H. Freed (Plenum, New York, 1979).
[12] A. Grupp and M. Mehring, in *Modern Pulsed and Continuous Wave Electron Spin Resonance*, edited by L. Kevan and M. K. Bowman (Wiley, New York, 1990).
[13] A. Schweiger, in *Advanced EPR*, edited by A. J. Hoff (Elsevier, Amsterdam, 1989).
[14] K. -P. Dinse, in *Advanced EPR*, edited by A. J. Hoff (Elsevier, Amsterdam, 1989).
[15] J. Gorcester and J. H. Freed, J. Chem. Phys. **85**, 5375 (1986).
[16] J. Gorcester and J. H. Freed, J. Chem. Phys. **88**, 4678 (1988).
[17] J. Gorcester and J. H. Freed, J. Magn. Reson. **78**, 291 (1988).
[18] J. Gorcester, S. Rananavare, and J. H. Freed, J. Chem. Phys. **90**, 5764 (1989).
[19] J. Gorcester, G. L. Millhauser, and J. H. Freed, in *Advanced EPR*, edited by A. J. Hoff (Elsevier, Amsterdam, 1989).
[20] J. Gorcester, G. L. Millhauser, and J. H. Freed, in *Modern Pulsed and Continuous Wave Electron Spin Resonance*, edited by L. Kevan and M. K. Bowman (Wiley, New York, 1990).
[21] J. H. Freed, J. Chem. Soc. Faraday Trans. **86**, 3173 (1990).
[22] M. K. Bowman, in *Modern Pulsed and Continuous Wave Electron Spin Resonance*, edited by L. Kevan and M. K. Bowman (Wiley, New York, 1990).
[23] D. Gamliel and J. H. Freed, J. Magn. Reson. **89**, 60 (1990).
[24] R. P. J. Merks and R. de Beer, J. Phys. Chem. **83**, 3319 (1979).
[25] J. Isoya, M. K. Bowman, J. R. Norris, and J. A. Weil, J. Chem. Phys. **78**, 1735 (1983).
[26] B. R. Patyal, R. H. Crepeau, D. Gamliel, and J. H. Freed, Chem. Phys. Lett. **175**, 445 (1990).
[27] B. R. Patyal, R. H. Crepeau, D. Gamliel, and J. H. Freed, Chem. Phys. Lett. **175**, 453 (1990).
[28] L. J. Schwartz, A. E. Stillman, and J. H. Freed, J. Chem. Phys. **77**, 5410 (1982).
[29] J. A. Goedkoop and C. H. MacGillavry, Acta Crystallogr. **10**, 195 (1957).
[30] H. M. McConnell, C. Heller, T. Cole, and R. W. Fessenden, J. Am. Chem. Soc. **82**, 766 (1960).
[31] R. C. McCalley and A. L. Kwiram (private communication).
[32] R. R. Ernst, G. Bodenhausen, and A. Wokaun, *Principles of Nuclear Magnetic Resonance in One and Two Dimensions* (Clarendon, Oxford, 1987).
[33] D. J. Schneider and J. H. Freed, Adv. Chem. Phys. **73**, 387 (1989).
[34] J. H. Freed and G. K. Fraenkel, J. Chem. Phys. **39**, 326 (1963).
[35] D. J. Schneider and J. H. Freed, in *Biological Magnetic Resonance*,

edited by L. J. Berliner and J. Reuben (Plenum, New York, 1989), Vol. 8.
[36] J. H. Freed, J. Phys. Chem. **71**, 38 (1967).
[37] W. B. Mims, in *Electron Paramagnetic Resonance*, edited by S. Geschwind (Plenum, New York, 1972).
[38] I. M. Brown, in *Time Domain Electron Spin Resonance*, edited by L. Kevan and R. N. Schwartz (Wiley, New York, 1979).
[39] K. M. Salikhov and Yu. D. Tsvetkov, in *Time Domain Electron Spin Resonance*, edited by L. Kevan and R. N. Schwartz (Wiley, New York, 1979).
[40] V. I. Popov, A. M. Raitsimring, K. M. Salikhov, and Yu. D. Tsvetkov, Sov. Phys. Solid State **20**, 985 (1978).
[41] There is another solid-state process known as "instantaneous diffusion" arising from the $S_{1z}S_{2z}$ interaction, which is not refocused in a spin echo when both spins S_1 and S_2 are "reversed" by, e.g., a π pulse (or in our case by the $\pi/2$ pulse) (Refs. 37–39). In principle this interaction will lead to coherence cross peaks in our SECSY-ESR spectra. [This is actually the exact analog of *jj* coupling in NMR which leads to coherence cross peaks in COSY and SECSY NMR (Ref. 32).] Since these are weak interactions that vary from one local site to another, they should appear as increased "broadenings" of the SECSY ESR along the ω_1 axis. However, spin diffusion and/or spin relaxation will modulate the frequency shift from this interaction in a random manner, and if rapid enough, would lead to the spectral diffusion processes noted above (Ref. 39). It is important to note that in our experiments with nonselective pulses, the usual distinction (Refs. 37–39) between like or *A* electron spins (which are excited by the pulse) vs unlike or *B* electron spins (which are not excited by the pulse) is moot, since *all* electron spins are rotated by the microwave pulses. Thus we must consider all the electron spins as *A* spins yielding coherence cross-peak broadening in the SECSY ESR in the limit of negligible spin and/or phonon dynamics, or alternatively as *B* spins (Ref. 39) in the limit of rapid spin and/or phonon dynamics.
[42] M. K. Bowman and L. Kevan, in *Time Domain Electron Spin Resonance*, edited by L. Kevan and R. N. Schwartz (Wiley, New York, 1979).
[43] D. Xu, R. H. Crepeau, and J. H. Freed (unpublished results).
[44] P. Höfer, A. Grupp, H. Nebenführ, and M. Mehring, Chem. Phys. Lett. **132**, 279 (1986).
[45] C. Gemperle, A. Schweiger, and R. R. Ernst, Chem. Phys. Lett. **178**, 565 (1991).
[46] J. H. Freed, Annu. Rev. Phys. Chem. **23**, 265 (1972).
[47] G. K. Fraenkel, J. Chem. Phys. **42**, 4275 (1965).
[48] A. G. Redfield, IBM J. Res. Dev. **1**, 19 (1957).
[49] A. Abragam, *Principles of Nuclear Magnetism* (Clarendon, Oxford, 1961), Chap. 8.